A reaction telegraph model reveals synergy between motility strategies in Myxococcus xanthus predation

Maxime Estavoyer

A reaction telegraph model reveals synergy between motility strategies in Myxococcus xanthus predation

Maxime Estavoyer[1]

[1] Inria, and Université de Lyon, Université Claude Bernard Lyon 1,
CNRS UMR 5208, Institut Camille Jordan, F-69603 Villeurbanne, France.

Abstract

The predatory bacterium *Myxococcus xanthus* can invade prey bacteria using two distinct motility apparatuses. It is commonly acknowledged that adventurous motility is used for isolated bacteria, while social motility corresponds to bacterial clusters. Inspired by recent biological findings, we propose a simple model of predatory invasion focusing on the co-occurrence of these two mechanisms and their possible synergistic effects. At microscopic scale, cell motion is persistent; therefore, we opt for a transport-reaction model, extending previous reaction-diffusion models. Another specificity is the structuration of the bacterial population into clusters with varying speeds and persistence times. In the linear regime, we find a transition from normal speed to anomalous speed, consistent with reaction-diffusion theory but with specificities due to the hyperbolic nature of the model. For the nonlinear regime, we numerically observe and study the existence of transitions between pulled and pushed fronts. Finally, we reproduced biological experiments with mutants lacking each of the motility apparatuses based on relevant modifications of the model. Moreover, we propose a rational basis for the reported synergistic effects. Our work paves the way for a better understanding of the complex waves of bacterial population advance, which are precursors to biofilm formation.

Introduction

Biology. *Myxococcus xanthus* is a social bacterium that moves and feeds cooperatively in predatory groups. *Myxococcus xanthus* bacteria employ two distinct modes of motility: social motility (S) and adventurous motility (A). Social motility is associated with the presence of type IV pili, which act as grappling hooks at the bacterial pole, promoting coordinated movement within clusters of bacteria [1]. Adventurous motility, on the other hand, involves gliding mechanisms that enable individual bacteria, mainly at the edge of the colony, to move [2]. These two motility systems, which depend on the expression of two distinct sets of genes [3], exhibit completely different characteristics which we will detail in the remainder of this article.

M. xanthus is a predatory bacterium, known to attack a wide variety of prey [4, 5]. The biomass released by the prey microorganisms is rich in amino acids and lipids, which constitute their main sources of carbon and energy. *Myxococcus xanthus* employs two attack strategies, choosing them based on the prey type [6]. The first strategy involves a frontal attack, where the predatory bacteria gradually penetrate the prey colony and progressively lyse the prey cells [7, 8]. In the other strategy, named *wolf pack*, *M. xanthus* cells surround the prey colony and undulate before killing it [8, 9]. In this article we focus on modeling the frontal attack.

The main mechanism of prey destruction results from contact-dependent killing by the bacteria. According to several recent studies, isolated bacteria of *Myxococcus xanthus* approach prey cells using their adventurous motility. Upon direct contact, they stop their movement and induce the death of the prey cell [10, 11, 12]. Cooperation among *Myxococcus xanthus* cells, as observed by Rosenberg et al., promotes vegetative growth and predation [13]. This cooperation enables a common secretion of hydrolytic enzymes, improving the efficiency of prey biomass degradation within a cluster, suggesting more efficient predation compared to individual cells [13]. In addition, Zhang et al. noted that isolated bacteria of *M. xanthus* frequently leave killed Escherichia coli prey without degrading the biomass, probably due to insufficient production of degrading enzymes [9, 11]. In the mathematical model we introduce, we assume that isolated bacteria lyse prey bacteria and leave the biomass behind. These nutrients will later be consumed by bacterial clusters.

These rod-shaped bacteria can move along their main axis thanks to their two motility

systems. At certain points, these bacteria reverse their direction by changing polarity [14]. Several studies have shown that *M.xanthus* is not chemotactic towards its prey [15], and whether the bacterium exhibits chemotactic behaviors in general remains controversial [16, 17]. Bacteria in bacterial clusters tend to be faster than isolated bacteria [18].

Since the pioneering works of Fisher [19] and Kolmogorov-Petrovskii-Piskunov [20], the dispersion of biological species is commonly modeled using reaction-diffusion equations. A major problem, in our case, with the choice of diffusion is that it does not model the persistence of motion [21]. In one dimension, and only in one dimension, the movement of the bacteria corresponds to a *Run and Tumble* process, also called *telegraph dispersal*, based on a velocity jump process [22, 23]. This choice is increasingly employed to model biological systems (see, for example, [24, 25, 26]), notably for modeling bacterial motility [27, 28, 29, 30].

In one dimension, during the *Run* phase, the particle moves in a straight line to the right or to the left at speed v. Then, after a random time interval, following a Poisson distribution, the particle undergoes a sudden stop and instantly reverses its direction. This movement is modeled by the following two kinetic equations,

$$\begin{cases} \partial_t f^+ + \dfrac{v}{\epsilon}\partial_x f^+ = \dfrac{1}{2\tau\epsilon}(f^- - f^+), \\ \\ \partial_t f^- - \dfrac{v}{\epsilon}\partial_x f^- = \dfrac{1}{2\tau\epsilon}(f^+ - f^-), \end{cases} \tag{1}$$

where f^+ (resp. f^-) corresponds to the density of bacteria moving to the right (resp. left). The parameter ϵ is a scaling parameter that represents the ratio between the spatial scale and the mean free path of bacteria. The transport term models the *Run* phase, while the RHS corresponds to the *Tumble* phase/ *Reversal* phase. Making the change of variable $f = f^+ + f^-$ and using the Kac trick [31], the system (1) simplifies into a single equation given by

$$\tau\epsilon^2\partial_{tt} + \partial_t f = \tau v^2 \partial_{xx} f. \tag{2}$$

When $\epsilon = 0$, equation (2) becomes the heat equation, $\partial_t f = D\partial_{xx} f$, where

$$D := \tau v^2. \tag{3}$$

This relation linking the diffusion coefficient, to the combination of persistence and instantaneous speed, is crucial in our study. The investigation of the mean square displacement (MSD) also enables the determination of relation (3) [23].

Model introduction.

The population of *M. xanthus* is structured into isolated bacteria and different clusters that interact with the nutrients present in the environment. The size of clusters is represented by the variable i, and we assume that the cluster size cannot exceed the size limit n, where n is a positive integer. The density of clusters of size i moving to the right is represented by the variable p_i^+, while the density of clusters of size i moving to the left is represented by the variable p_i^-. We also denote p_i as the density of bacterial clusters of size i, defined by $p_i := p_i^+ + p_i^-$.

The densities p_1^+ and p_1^- are given by the following system of equations,

$$\begin{cases} \partial_t p_1^+ + \dfrac{1}{\epsilon}\partial_x p_1^+ = \dfrac{1}{2\epsilon^2}(p_1^- - p_1^+) + \mathcal{F}_1^+[p_j^\pm] + \mathcal{C}_1^+[p_j^\pm] + \dfrac{\alpha_1 p_1 (1-p)_+}{2}, \\ \\ \partial_t p_1^- - \dfrac{1}{\epsilon}\partial_x p_1^- = \dfrac{1}{2\epsilon^2}(p_1^+ - p_1^-) + \mathcal{F}_1^-[p_j^\pm] + \mathcal{C}_1^-[p_j^\pm] + \dfrac{\alpha_1 p_1 (1-p)_+}{2}, \end{cases} \tag{4}$$

with, p the total number of bacteria given by the following formula, $p := p_1 + 2p_2 + \ldots + np_n$ and $(1-p)_+$ corresponding to the positive part of $1-p$, $(1-p)_+ := \max\{1-p, 0\}$.

By a scaling of the time and space, which we do not detail in this document, the coefficients corresponding to the instantaneous speed and persistence of isolated bacteria are chosen equal to 1. The operator $\mathcal{F}_i^\pm[p_j^\pm]$ represents the fragmentation events associated with bacterial clusters of size i moving to the right (+) or to the left (-) between times t and $t + \mathrm{d}t$. This operator is given in general form by the following equality

$$\mathcal{F}_i^\pm[p_j^\pm] = \frac{1}{2} \times 2 \sum_{j=i+1}^{n} \beta(j)\eta(j,i)p_j - \beta(i)p_i^\pm, \qquad i \in \{1, \ldots, n\},$$

where $\beta(i)$ represents the fragmentation rate of clusters of size i. The first sum represents larger clusters that have fragmented into two distinct parts, with one resulting cluster having size i. We assume that when a cluster of bacteria fragments, the two daughter clusters randomly choose their direction, either to the right or to the left. In this sum, the function η corresponds to the fragmentation kernel; in other words, $\eta(j,i)$ represents the probability that a cluster of size j fragments into a cluster of size i and a cluster of size $j-i$. The second term of the fragmentation term corresponds to clusters of size i that have fragmented during the time interval $\mathrm{d}t$. In this article, we make the following assumptions

$$\beta(j) = \beta \times j, \qquad \text{and,} \qquad \eta(j,i) = \frac{1}{j-1}, \quad \text{for all } i \in \{1, \ldots, j-1\}.$$

We assume that the larger a cluster is in size, the more likely it is to undergo fragmentation. Regarding possible fragmentation events, we assume them to be uniformly probable.

The operator $\mathcal{C}_i^{\pm}[p_j^{\pm}]$ corresponds to the coagulation events during the time interval $\mathrm{d}t$, and it is given by the following formula

$$\mathcal{C}_i^{\pm}[p_j^{\pm}] = \frac{1}{2}\sum_{j=1}^{i-1}\gamma(i-j,j)\left[p_j^{\pm}p_{i-j}^{\pm} + \frac{1}{2}(p_j^{+}p_{i-j}^{-} + p_j^{-}p_{i-j}^{+})\right] - p_i^{\pm}\sum_{j=1}^{n-i}\gamma(j,i)p_j, \quad i \in \{1,\dots,n\}.$$

The first term corresponds to the coagulation event of two clusters of smaller sizes forming a cluster of size i. Here, we assume that if two clusters are moving in the same direction, the resulting cluster from their coagulation will also move in the same direction. When two clusters coagulate but are not moving in the same direction, in this case, the newly formed cluster has an identical probability of moving either to the right or to the left. The function $\gamma(i-j,j)$ represents the probability that a cluster of size j coagulates with a cluster of size $i-j$. We assume that the function γ is given by

$$\gamma(j,j') = \gamma \times j \times j', \qquad \text{for all } j,j' \in \{1,\dots,n\} \text{ such that } j+j' \leq n.$$

The second term of the coagulation operator represents all clusters of size i that have coagulated with another cluster to form a larger-sized cluster. The fragmentation and coagulation operators preserve the mass, p.

Finally, we model the division of isolated bacteria. When an isolated bacterium divides, we assume that the two daughter bacteria will also be isolated. The parameter α_1 corresponds to the proliferation rate. As the mass p increases, the proliferation term decreases. When the mass exceeds a threshold, we assume that division events are no longer possible.

For clusters of size $i \in \{2,3,\dots,n\}$, the equations of the couple (p_i^{+}, p_i^{-}) are given by

$$\partial_t p_i^{\pm} \pm \frac{v(i)}{\epsilon}\partial_x p_i^{\pm} = \pm\frac{1}{2\tau(i)\epsilon^2}(p_i^{-}-p_i^{+}) + N\left[d(i-1)p_{i-1}^{\pm} - d(i)p_i^{\pm}\right](1-p)_+ + \mathcal{F}_i^{\pm}[p_j^{\pm}] + \mathcal{C}_i^{\pm}[p_j^{\pm}], \quad (5)$$

where N is a spatiotemporal variable corresponding to the nutrient density.

These equations have the same coagulation and fragmentation terms as the equations (4). The division term is now given by the term

$$\text{Division term:} \quad N \times \left[d(i-1)p_{i-1}^{\pm} - d(i)p_i^{\pm}\right] \times (1-p)_+.$$

The nutrients are created by prey lysis. We assume that N is governed by the following equation,

$$\partial_t N = \delta p_1 (1 - N/N_M), \tag{6}$$

with δ the rate of nutrient creation and N_M the carrying capacity. We assume that the diffusion of these nutrients is negligible. These nutrients created by the predation of isolated adventurous bacteria will, in proportion to the nutrient presence, enable the division of bacteria within bacterial clusters. In this equation, we assume that the effect of bacteria on prey depends on the size of the clusters. Isolated bacteria kill the prey, creating nutrients, while the clusters consume these nutrients to increase their division rate. Since we focus solely on the invasion phenomenon, we do not model the degradation of these nutrients by bacterial clusters.

We assume, in this division term, that when a bacterium divides within a cluster, the two daughter bacteria remain part of the same cluster. Thus, the evolution of clusters of size i between times t and $t + \mathrm{d}t$ will depend on clusters of size $i - 1$ and size i for which a bacterium will divide. We assume that the division rate, d, is given by the following formula

$$d(i) = i \times \alpha_2, \qquad \text{for all } i \in \{2, \dots n-1\}, \quad \text{and} \quad d(1) = d(n) = 0.$$

The linear growth of the function d represents the fact that every bacteria, whether in a cluster or not, has the same chance of dividing. Consequently, the larger a cluster is, the more likely one of its bacteria will divide. To ensure that the maximum size of bacterial clusters is equal to n, we assume that bacteria can no longer divide within clusters of size n. Again, we assume that the division rate decreases with respect to the total mass, p, and is only possible if the mass is below the critical mass of 1.

The function $v : i \in \{2, \dots, n\} \longmapsto v(i)$ represents the instantaneous speed of bacterial clusters of size i relatively to the isolated bacteria and the function $\tau : i \in \{2, \dots, n\} \longmapsto \tau(i)$ represents the average time between a change of direction relatively to the isolated bacteria. For the equations related to the clusters, we assume that the scaling parameter is the same as for the isolated bacteria equations, ϵ.

Mathematical literature. The model (4)-(5)-(6) corresponds to an extension of the model presented in the article by Calvez et al. [32]. In the article [32], the authors introduce a simplified reaction-diffusion model that only considers isolated bacteria and clusters of two bacteria.

Their goal was to study the impact of the speed advantage of bacterial clusters. Through numerical simulations, the authors highlight the presence of pulled and pushed fronts. Moreover, in the article [33], the authors have demonstrated that under the assumption of fast coagulation-fragmentation, there is a unique transition between pulled and pushed fronts. In the present article, we enhance this model in several aspects. Firstly, we model bacterial clusters of size greater than 2. Then, for the reasons described above, we favor a telegraph dispersal rather than the previous diffusion operator. We also decide to model the creation of nutrients resulting from the lysis of prey bacteria by isolated predator bacteria, as well as the effect of these nutrients on the proliferation of bacterial clusters. Other, older models have been introduced to model the spread of the *M. xanthus* bacteria [34, 35]. However, these models do not consider the predatory nature of the bacteria and the coexistence of the two motility systems. The study of traveling waves for reaction-telegraph equations has already been studied in numerous articles (See for example [36, 37, 38, 39, 40, 41, 42, 43]) and for more general systems of several hyperbolic equations [44, 45].

Results. In this article, we focus on the linear and nonlinear speeds of the model (4)-(5)-(6). When the nonlinear speed equals the linear speed, the front is said to be pulled. Conversely, when the linear speed differs from the nonlinear speed, the front is pushed [46]. Based on the marginal stability conjecture and under certain assumptions, we propose a formula for the linear speed. Two scenarios are possible: either the linear speed equals the linear speed of the two-equation system (4), decoupled from the other equations; or the linear speed is greater than this speed, in which case the propagation is termed anomalous. To the best of our knowledge, no article reports such a phenomenon for hyperbolic equations. We also perform numerical simulations to determine the nonlinear speed of the model. Our numerical results reveal the existence of both a pulled front regime and a pushed front regime. In our numerical experiments, for the pushed front regime, the nonlinear speed consistently exceeds the linear speed.

Myxococcus xanthus has two strains $A+S-$ and $A-S+$ corresponding respectively to a population of *Myxococcus xanthus* bacteria composed solely of adventurous bacteria and another composed solely of social bacteria. According to the results of biological experiments presented in the article [12], the *Wildtype* strain (or $A+S+$) and the $A+S-$ strain significantly invade the *E.*

coli prey much faster than the $A-S+$ strain. Based on our model, we propose two mathematical systems corresponding respectively to the $A+S-$ and $A-S+$ strains. Our numerical simulations yield results consistent with the biological experiments, showing that the $A-S+$ strain has great difficulty invading the prey.

Finally, we investigate, through numerical simulations, the impact of the existence of both motility systems on the invasion speed. To achieve this, we use the relation (3) linking the diffusion coefficient with persistence and instantaneous speed. This allows us to study the invasion speed for various parameter values $(\tau(i), v(i))$ under the constraint $1 = \tau(i)v^2(i)$ for all $i \in \{2, \dots, n\}$. According to our numerical simulations, the characteristics induced by the coexistence of adventurous and social motility systems significantly facilitate the predation of a prey bacteria.

Outline. The document is organized as follows: In Section 1 we first study the simplified system, $n = 2$, where only isolated bacteria and pairs of bacteria are considered. We first derive the linear speed of the model. Subsequently, followed by an exploration of the nonlinear speed through numerical simulations. Finally, we conclude this section by describing results related to the biological modeling of this problem. In Section 2, we extend this analysis to the more general case where $n > 2$, applying similar methods to investigate the behavior of the extended model.

1 Simplified case $n = 2$

In this section, we assume that clusters can only contain two bacteria. According to the biological experimental data presented in the article [47], there is a symmetry between the probability of fragmentation and coagulation. To simplify the calculations presented in this section, we assume that the fragmentation rate equals the coagulation rate, and denote it by k.

Under the assumption $n = 2$, the model (4)-(5)-(6) becomes the following,

$$\begin{cases} \partial_t p_1^+ + \dfrac{1}{\epsilon}\partial_x p_1^+ = \dfrac{1}{2\epsilon^2}(p_1^- - p_1^+) - k(p_1^+)^2 - kp_1^+ p_1^- + kp_2 + \dfrac{\alpha_1}{2} p_1(1-p)_+, \\ \partial_t p_1^- - \dfrac{1}{\epsilon}\partial_x p_1^- = \dfrac{1}{2\epsilon^2}(p_1^+ - p_1^-) - k(p_1^-)^2 - kp_1^+ p_1^- + kp_2 + \dfrac{\alpha_1}{2} p_1(1-p)_+, \\ \partial_t p_2^+ + \dfrac{v}{\epsilon}\partial_x p_2^+ = \dfrac{1}{2\tau\epsilon^2}(p_2^- - p_2^+) - kp_2^+ + \dfrac{k}{2}(p_1^+)^2 + \dfrac{k}{2} p_1^+ p_1^-, \\ \partial_t p_2^- - \dfrac{v}{\epsilon}\partial_x p_2^- = \dfrac{1}{2\tau\epsilon^2}(p_2^+ - p_2^-) - kp_2^- + \dfrac{k}{2}(p_1^-)^2 + \dfrac{k}{2} p_1^+ p_1^-, \\ \partial_t N = \delta p_1(1 - N/N_M). \end{cases} \tag{7}$$

The choice of the term modeling bacterial proliferation is specifically motivated for values of n strictly greater than 2. When $n = 2$, this term becomes irrelevant. Indeed, in the system of equations (7), clusters of two bacteria gradually disappear, and nutrients do not influence the predation behavior of *M. xanthus*. To overcome this problem, we add a nonlinear, nutrient-dependent logistic proliferation term into the equations governing the two-bacteria clusters.

$$\begin{cases} \partial_t p_1^+ + \dfrac{1}{\epsilon}\partial_x p_1^+ = \dfrac{1}{2\epsilon^2}(p_1^- - p_1^+) - k(p_1^+)^2 - kp_1^+ p_1^- + kp_2 + \dfrac{\alpha_1}{2} p_1(1-p)_+, \\ \partial_t p_1^- - \dfrac{1}{\epsilon}\partial_x p_1^- = \dfrac{1}{2\epsilon^2}(p_1^+ - p_1^-) - k(p_1^-)^2 - kp_1^+ p_1^- + kp_2 + \dfrac{\alpha_1}{2} p_1(1-p)_+, \\ \partial_t p_2^+ + \dfrac{v}{\epsilon}\partial_x p_2^+ = \dfrac{1}{2\tau\epsilon^2}(p_2^- - p_2^+) - kp_2^+ + \dfrac{k}{2}(p_1^+)^2 + \dfrac{k}{2} p_1^+ p_1^- + \dfrac{\alpha_2}{2} N p_2 \,(1-p)_+ \,, \\ \partial_t p_2^- - \dfrac{v}{\epsilon}\partial_x p_2^- = \dfrac{1}{2\tau\epsilon^2}(p_2^+ - p_2^-) - kp_2^- + \dfrac{k}{2}(p_1^-)^2 + \dfrac{k}{2} p_1^+ p_1^- + \dfrac{\alpha_2}{2} N p_2 \,(1-p)_+ \,, \\ \partial_t N = \delta p_1(1 - N/N_M). \end{cases} \tag{8}$$

Such a choice would be irrelevant for a larger n. The parameter v (resp. τ) represents the advantage or disadvantage in speed (resp. average time before a change of direction) of clusters of two bacteria.

1.1 Linear speeds

In this section, we study the critical linear propagation speed of the model (8). Linearizing this model around the zero equilibrium point gives us the following linear model:

$$\begin{cases} \partial_t p_1^+ + \dfrac{1}{\epsilon}\partial_x p_1^+ = \dfrac{1}{2\epsilon^2}(p_1^- - p_1^+) + kp_2 + \dfrac{\alpha_1}{2}p_1, & \text{(9a)} \\ \partial_t p_1^- - \dfrac{1}{\epsilon}\partial_x p_1^- = \dfrac{1}{2\epsilon^2}(p_1^+ - p_1^-) + kp_2 + \dfrac{\alpha_1}{2}p_1, & \text{(9b)} \\ \partial_t p_2^+ + \dfrac{v}{\epsilon}\partial_x p_2^+ = \dfrac{1}{2\tau\epsilon^2}(p_2^- - p_2^+) - kp_2^+, & \text{(9c)} \\ \partial_t p_2^- - \dfrac{v}{\epsilon}\partial_x p_2^- = \dfrac{1}{2\tau\epsilon^2}(p_2^+ - p_2^-) - kp_2^-. & \text{(9d)} \end{cases}$$

Note that equations (9c)-(9d) are independent of the variables p_1^+ and p_1^-. However, the variables $p_2^\pm$, through the coupling term, influence the behavior of the variables $p_1^\pm$. Nevertheless, the variables $p_2^\pm$ decay exponentially to zero at every point for all x as $t \to \infty$. Thus, one might expect that the coupling term in equations (9a)-(9b) would quickly stop affecting the propagation speed of the traveling wave solutions of p_1. However, we will see that the coupling term can irreversibly increase the wave speed. This type of phenomenon, called *anomalous propagation*, was first introduced in the article [48] and has since been theoretically studied by numerous authors [49, 50, 51, 52].

There are therefore two possibilities concerning the linear propagation speed of (9a)-(9d). In the first case, the coupling term has no effect, and the critical asymptotic speed is determined solely by the decoupled system of equations (9a)-(9b), i.e., with $k = 0$. In this case, we will use the term *normal speed*. Conversely, when the pairs of bacteria, through the coupling term, influence the speed of the isolated bacteria, we will refer to it as *anomalous speed*.

We define the linear propagation speed as follows:

Definition 1 (Linear propagation speed)**.** *The linear propagation speed of a linear system (S) is given by*

$$s^\star_{lin} = \sup\{s :\ D_s(\nu, \lambda) \text{ has a pinched double root with } \operatorname{Re}\lambda \geq 0\},$$

where $D_s(\nu, \lambda)$ is the dispersion relation associated with the problem (S), and the notion of a pinched double root is introduced in the appendix A.

This definition is based on the distinction between convective instability and absolute instability [49]. In certain specific cases, this definition may prove to be imperfect. It then becomes

necessary to consider the singularities of the pointwise Green's function associated with the problem. The connection between pinched double roots and these singularities has been studied theoretically for a broad class of parabolic systems, by Holzer and Scheel in the article [49]. However, to simplify the calculations in Appendix A, we will nonetheless use this definition.

In Appendix A, we show that the linear propagation speed, $s^{\star}_{\text{lin}}$, can take one of four possible values:

- The two *normal speeds*: parabolic and hyperbolic

$$s_{\text{para}} := \frac{2\sqrt{\alpha_1}}{1+\alpha_1\epsilon^2}, \qquad s_{\text{hyp}} := \frac{1}{\epsilon}.$$

- The two *positive anomalous speeds* given by:

$$(s^{\pm}_{\text{anom}})^2 = s^{\pm}(0) = \frac{-a_2(0) \pm \sqrt{a_2^2(0) - 4a_0(0)a_4}}{2a_4},$$

  provided these two speeds are well defined. The functions a_0, a_2, and the coefficient a_4 are defined by equations (A.9), (A.10), and (A.11), respectively, in Appendix A.

By definition 1, the selection principle among these possible linear speeds corresponds to the maximum of those that are indeed associated with pinched double roots. Based on this postulate, it is possible to explicitly calculate certain critical transition values, which will not be detailed in this article due to their significant complexity. We illustrate transitions between different possible linear speeds in Figure A.1.

When isolated bacteria are faster than clusters, we obtain the following result:

- If $\epsilon < 1/\sqrt{\alpha_1}$, then the linear propagation speed can be the parabolic speed or one of the anomalous speeds: s_{para}, s^{+}_{anom}, and s^{-}_{anom}.

- If $\epsilon > 1/\sqrt{\alpha_1}$, then the linear propagation speed corresponds to the hyperbolic speed.

In Appendix A, we also verify through numerical simulations that this linear propagation speed is indeed selected for a nonlinear model in a pulled front regime, when initial conditions correspond to Heaviside functions.

1.2 Nonlinear speed – Pulled and Pushed regime

The speed of the nonlinear model (8) is not necessarily equal to the linear propagation speed. In this section, we use numerical simulations to compare the nonlinear and linear speeds to determine whether the front is pulled or pushed [46].

For numerical simulations, we employ the numerical scheme presented in the article [42], which is based on the nonlinear flux-limiter schemes developed in the articles [53, 54]. To approximate the wave speed, we use an algorithm based on the LeVeque-Yee formula [55, 56]. In this work, we consider only steep initial data. More specifically, for the model (8), we consider initial conditions of the form $p_i^{\pm}(t=0,x) = (p_i^{\star}/2)H(x-x_0)$, for $i=1,2$, where H denotes the Heaviside function and x_0 is a positive constant.

In Figure 1, we plot with black dots, for different values of parameter v, the evolution of the critical speed for the nonlinear model normalized by the speed we obtain when $v=1$. For $v=1$, the selected numerical speed corresponds well to the parabolic speed. However, a slight numerical error on the order of 10^{-2} remains due to the inaccuracies of the numerical simulations (mesh, convergence time, etc.). Since this error persists for other values of v, we have chosen to normalize the results by the value calculated at $v=1$ in order to improve the readability of the figure and the comparison with theoretical speeds. The colored curves correspond to the linear propagation speed normalized by the parabolic speed independent of v. We observe two different scenarios separated by a critical threshold v_c. When $v < v_c$, the front is pulled; indeed, the selected numerical speed corresponds to the parabolic linear speed. However, when v becomes greater than the critical threshold v_c, the speed becomes greater than the parabolic linear speed and also greater than all possible linear speeds. Therefore, the front is pushed for $v > v_c$. The hyperbolic speed and the anomalous plus speed are not represented in this figure as they are not admissible for the chosen parameter values.

We performed several additional numerical simulations, not presented in this article, for different parameter values. According to these simulations, it seems that the speed of the nonlinear model can be equal to the parabolic and hyperbolic linear speeds but never equals either of the two anomalous linear speeds. For the model associated with diffusion, numerical results presented in the articles [32, 33] also show these same results. Moreover, when the model is in the pushed regime, the propagation speed appears to always be greater than the linear speed. For

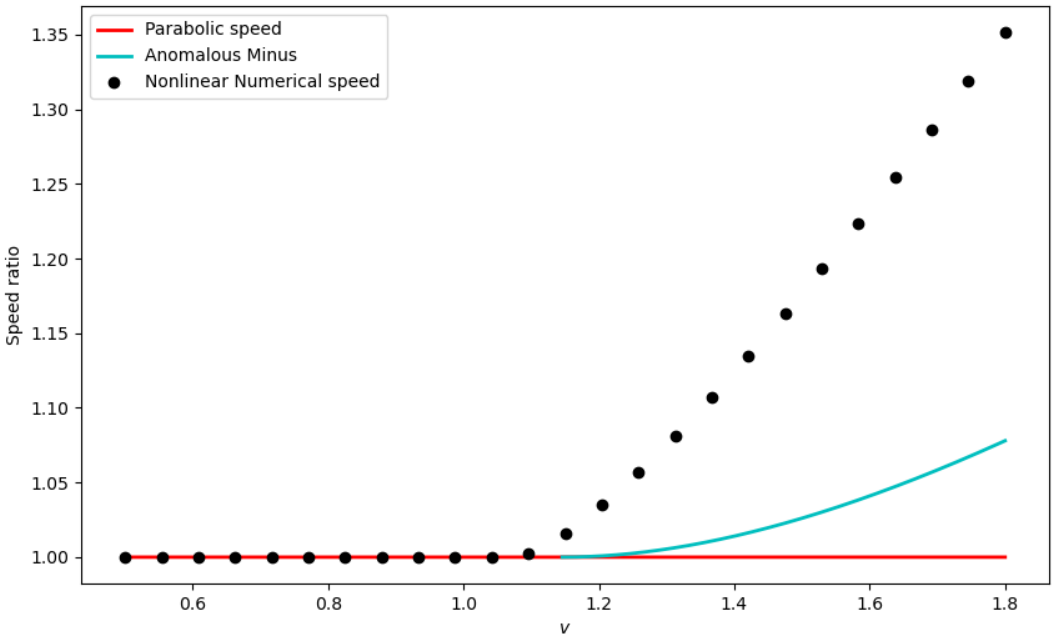

Figure 1: **Comparison between the numerical critical speed of the model** (8) **and the theoretical linear speed for different values of parameter** v**.** The black points correspond to the numerical critical speed of the model (8) normalized by the speed for $v = 1$. The red curve represents the parabolic speed, and the cyan curve represents the anomalous minus speed. For v small enough, the critical speed corresponds to the parabolic speed, indicating a pulled front regime. For $v > v_c \approx 1.1$, the critical speed differs from the possible linear speeds, indicating a pushed front regime. The other parameter values are given by $k = 1$, $\alpha_1 = 1$, $\alpha_2 = 4$, $\tau = 1$, $N_M = 6$, $\epsilon = 0.9$, and $\delta = 2$.

single reaction-diffusion equations, the nonlinear speed is always greater than the linear speed; however, in the article [57], the authors presented a counterexample showing that this is not always the case for reaction-diffusion systems.

1.3 Optimal invasion strategy

The difference in motility between isolated bacteria and bacterial clusters leads to distinct characteristics regarding their persistence and instantaneous speed. In the article [18], it was shown that bacterial clusters move faster than isolated bacteria. Moreover, based on the contrasting mechanisms of adventurous and social twitching motility [58, 59], we decided to test the case where A motility is more persistent than the other. Therefore, we assume that parameter values are $v > 1$ and $\tau < 1$.

In Figure 2, using numerical simulations, we look at the critical speed of the model (8) as a function of the values of the couple of parameters linked to the motion characteristics (v, τ). Once again, we normalize this numerical critical speed by the speed calculated at $v = 1$ and $\tau = 1$. When $v = 1$ and $\tau = 1$, the front is pulled, and the selected linear speed is the parabolic speed. The intensity of the red color represents the renormalized numerical critical speed. We observe that as either v or τ increases, this speed also increases. Since the instantaneous speed advantage of clusters is offset by a persistence disadvantage, it is also important to study the evolution of the critical speed as one parameter increases and the other decreases.

As mentioned in the introduction, the diffusion coefficient is a combination of persistence and instantaneous speed (3). We denote by D the ratio between the coefficient of diffusion associated with bacterial clusters and the diffusion coefficient of isolated bacteria. To focus exclusively on the impact of differences in instantaneous speed and persistence time between clusters and isolated bacteria, we assume that this ratio is equal to 1, i.e., $D := \tau v^2 = 1$. If this ratio differs from 1, for example $D > 1$, this difference could alone influence the propagation speed of the bacteria [32, 33]. We thus define $\mathbf{s}$ as the nonlinear critical speed of the model (8), under the constraint $1 = \tau v^2$,

$$\mathbf{s}(\tilde{v}) = s^\star(\tau = 1/\tilde{v}^2, v = \tilde{v}),$$

with $s^\star$ the critical nonlinear speed of traveling wave solution of (8).

In Figure 3, we plot, for two parameter values α_1, the variations of the speed $\mathbf{s}$. Firstly, we

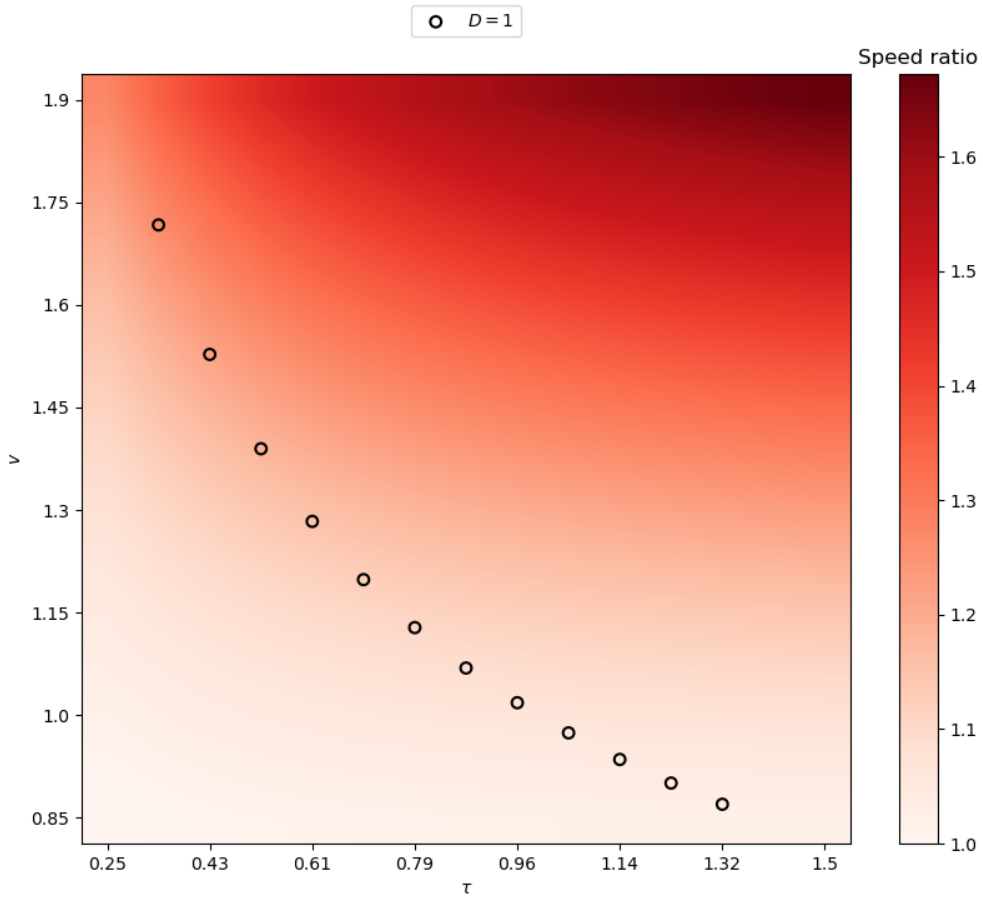

Figure 2: **Evolution of the numerical critical speed of the travelling wave as a function of the parameters τ and v for the model** (8). The colorimetry represents the intensity of the numerical critical speed obtained from our numerical simulations, divided by the speed at $\tau = 1$ and $v = 1$ (parabolic speed). The circles correspond to the constraint $D := \tau v^2 = 1$. We note that under the constraint $\tau v^2 = 1$, the increase of v and the decrease of τ leads to an increase in the speed ratio. The parameter values are: $\alpha_1 = 0.5$, $\alpha_2 = 4$, $k = 1$, $\epsilon = 0.85$, $\delta = 3$, $N_M = 6$.

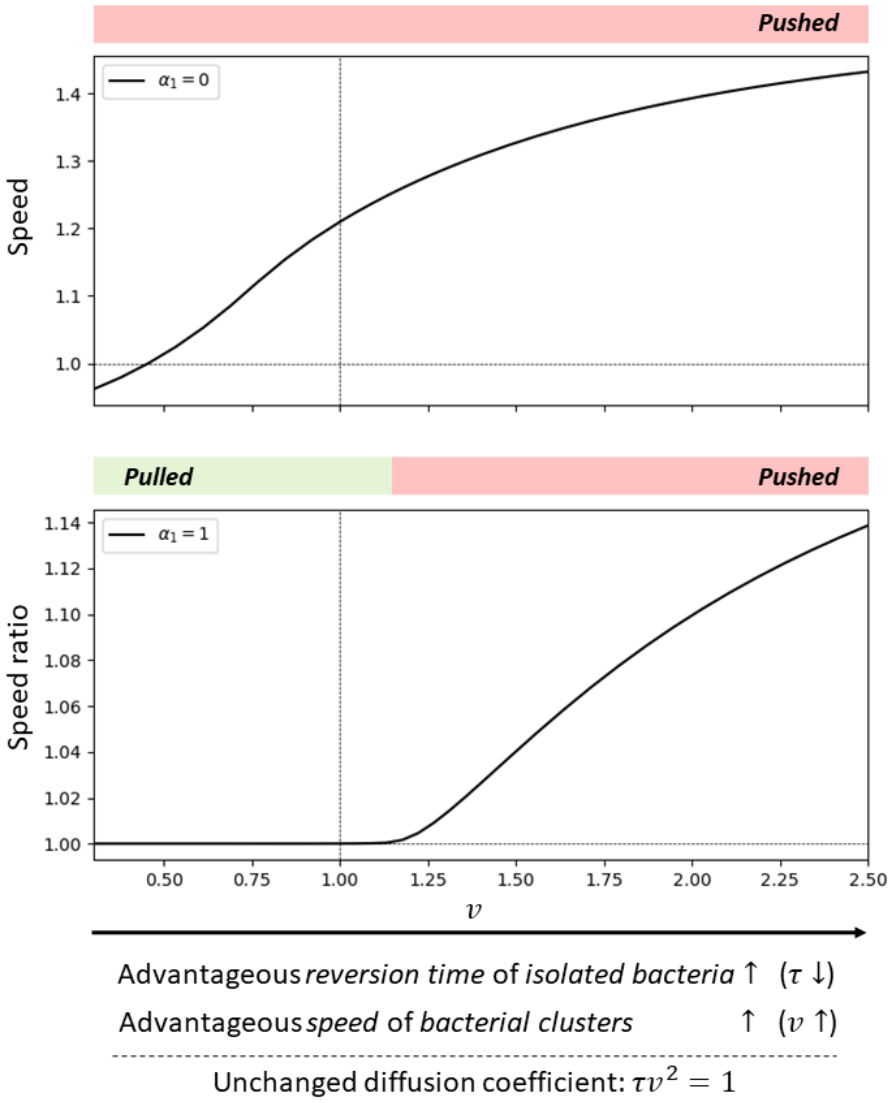

Figure 3: **Evolution of the numerical critical speed of the model** (8) **under the constraint** $1 = \tau v^2$ **for: Top.** $\alpha_1 = 0$**, Bottom.** $\alpha_1 = 1$**.** The black curves represent the numerical nonlinear speed of the model (8). For the bottom figure, we normalize this numerical speed by the speed calculated at $\tau = 1$ and $v = 1$ (parabolic speed). We calculate this speed for different values of v under the constraint $1 = \tau v^2$, so as v increases, the value of the parameter τ, not shown in the figure, will decrease. The rectangles above the two figures illustrate the pushed or pulled regime of the traveling wave. We observe that in both cases, the increase in v coupled with the decrease in τ leads to an increase in the critical speed. The values of the other parameters are given by $\alpha_2 = 4$, $k = 1$, $\epsilon = 0.85$, $N_M = 3$ and $\delta = 2$.

assume the extreme case where the division rate of isolated bacteria is zero, which is mathematically expressed as $\alpha_1 = 0$. In this case, we observe that the speed $\mathbf{s}$ is strictly increasing as v increases (and as τ decreases) under the constraint $1 = \tau v^2$. Under the assumption $\alpha_1 = 0$, we lose the linear proliferation term of isolated bacteria, so propagation can only occur through the nonlinear terms.

In the case $\alpha_1 = 1$, we observe two possible scenarios. When v is small enough, the front is pulled, and the critical nonlinear speed always corresponds to the normal critical nonlinear speed in the case $v = 1$ and $\tau = 1$. Indeed, according to our numerical simulations, it is impossible to select an anomalous speed. When v becomes large enough, the front becomes pushed, and the increase in v under the constraint $1 = \tau v^2$ leads to an increase in invasion speed. In this figure, the critical transition between pulled and pushed fronts is close to the value $v_c \approx 1.1$ ($\tau_c = 1/v_c^2$). This critical threshold strongly depends on the parameter values.

More generally, according to our numerical simulations, for $\alpha_1 > 0$, there exists v_c such that: if the advantage of instantaneous speed coupled with the disadvantage of persistence is sufficiently small, i.e., $v < v_c$, the invasion speed is not affected by this difference in speed and persistence. In such a case, the coexistence of both motility systems would not impact the propagation speed of the bacteria. However, if the instantaneous speed v becomes greater than the critical threshold v_c (resulting in $\tau < \tau_c$), in this case, the advantage of clusters leads to an increase in the invasion speed. Thus, the coexistence of both motility systems, adventurous and social, would be a significant advantage for predation.

2 Extended model $n > 2$.

In this extended model, the spatially homogeneous null state remains an unstable equilibrium point. The stable steady state is more complex to characterize explicitly, and we use numerical simulations to determine it.

2.1 Linear speed

By applying a reasoning similar to the case $n = 2$, by Definition 1, we show in Appendix B that the linear propagation speed, $s^\star_{\text{lin}}$, can take the following possible values:

- The two normal speeds: parabolic and hyperbolic

$$s_{\text{para}} := \frac{2\sqrt{\alpha_1}}{1+\alpha_1\epsilon^2}, \qquad s_{\text{hyp}} := \frac{1}{\epsilon}.$$

- The different anomalous speeds: $s^{\pm}_{\text{anom},i}$ for all $i \in \{2,\dots,n\}$, where $s^{\pm}_{\text{anom},i}$ are defined in equation (B.3).

2.2 Nonlinear speed – Pulled and Pushed regime

In Figure 4, using numerical simulations, we plot, with black dots, the evolution of the critical speed for the nonlinear model (4)-(5)-(6) for different functions v. More precisely, we define v as a threshold function of the following form $v(i) = \mathbf{1}_{i<\lfloor n/2\rfloor}(i) + \bar{v}\mathbf{1}_{i\geq\lfloor n/2\rfloor}(i)$, for all $i \in \{2,\dots,n\}$, with $\bar{v}$ a positive real parameter that we vary in Figure 4. For the same reasons as before, we normalize the numerical speed by the speed obtained at $\bar{v} = 1$. To compare with theoretical linear speeds, we also illustrate the parabolic speed by the red curve and the largest of the admissible anomalous speeds by the blue curve, both normalized by the parabolic speed. When $\bar{v}$ is small enough, the speed of the system (4)-(5)-(6) equals the linear prediction. However, when $\bar{v}$ becomes sufficiently large, the speed surpasses the linear speeds, and the front becomes pushed.

2.3 Biological modeling

2.3.1 Propagation example

In Figure 5, we illustrate the traveling wave solution of the model with multiple cluster sizes (4)-(5)-(6). Dotted lines represent the density of clusters of different sizes multiplied by their size at a given time T. The propagation speeds associated with the densities p_i, with $i \in \{1,\dots,n\}$, are always similar. The grey area corresponds to the nutrient density at the same time. Upstream of the front, we only observe the presence of isolated bacteria represented by the black line. These isolated bacteria generate nutrients that subsequently allow the invasion of bacteria clusters. The different cluster sizes are indicated by the following colorimetry: from blue ($i = 2$) to red ($i = n$). We note that the invasion of clusters of different sizes occurs in a staggered and ordered manner based on their size. After isolated bacteria, we observe the emergence of clusters of two bacteria, then clusters of three bacteria, and so on. This heterogeneity is also observed

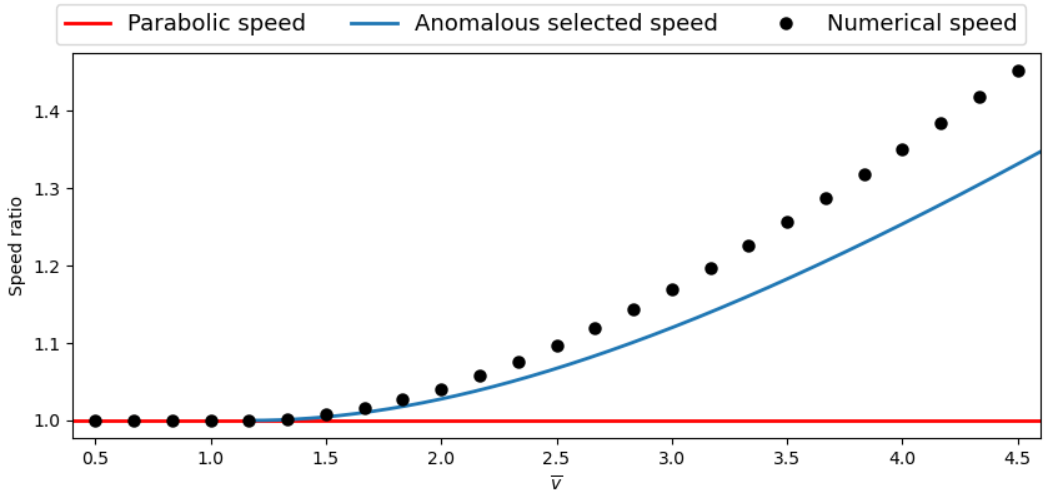

Figure 4: **Comparison between the numerical critical speed of the nonlinear model (4)-(5)-(6) and the theoretical linear speed for different values of the parameter $\bar{v}$.** The black points correspond to the numerical critical speed of the nonlinear model (4)-(5)-(6) normalized by the speed for $\bar{v} = 1$. The red horizontal line represents the parabolic linear speed, and the blue curve represents the largest admissible anomalous speeds, both normalized by the parabolic speed. For $\bar{v}$ small enough, the critical speed of the nonlinear model is equal to the linear speed. Then, when $\bar{v}$ becomes large enough, the nonlinear speed becomes strictly greater than the linear speed. The values of the other parameters are given by $\beta = \gamma = \alpha_1 = \alpha_2 = N_M = 1$, $n = 4$, $\epsilon = 0.95$, $\delta = 1.5$, and the functions are given by $\tau(i) = 1$ for all $i \in \{1, 2, 3, 4\}$, $v(2) = 1$.

in biological predation experiments with the bacteria *M. xanthus* [47]. Indeed, at the forefront of the predation front, there are mainly isolated bacteria, called *scouts*. Following this group, clusters of small size, called *loners*, appear. Finally, in the wake of these clusters, the invasion of large clusters, called *swarms*, occurs.

2.3.2 Study of strain invasion speed

In the article [12], the authors investigated the invasion speed of three strains, *Wildtype* ($A+S+$), $A+S-$, and $A-S+$. The *Wildtype* strain has both motility apparatuses, A and S, while the other strains are mutants that have lost one of these systems: the $A+S-$ strain has lost the S apparatus, and the $A-S+$ strain has lost the A apparatus. To do this, the authors conducted three similar predation experiments, one for each strain, which they stopped at the same time to analyze the progress of the bacterial invasion. Their results show that the $A-S+$ strain has significant difficulty invading the prey compared to the *Wildtype* and $A+S-$ strains. In this

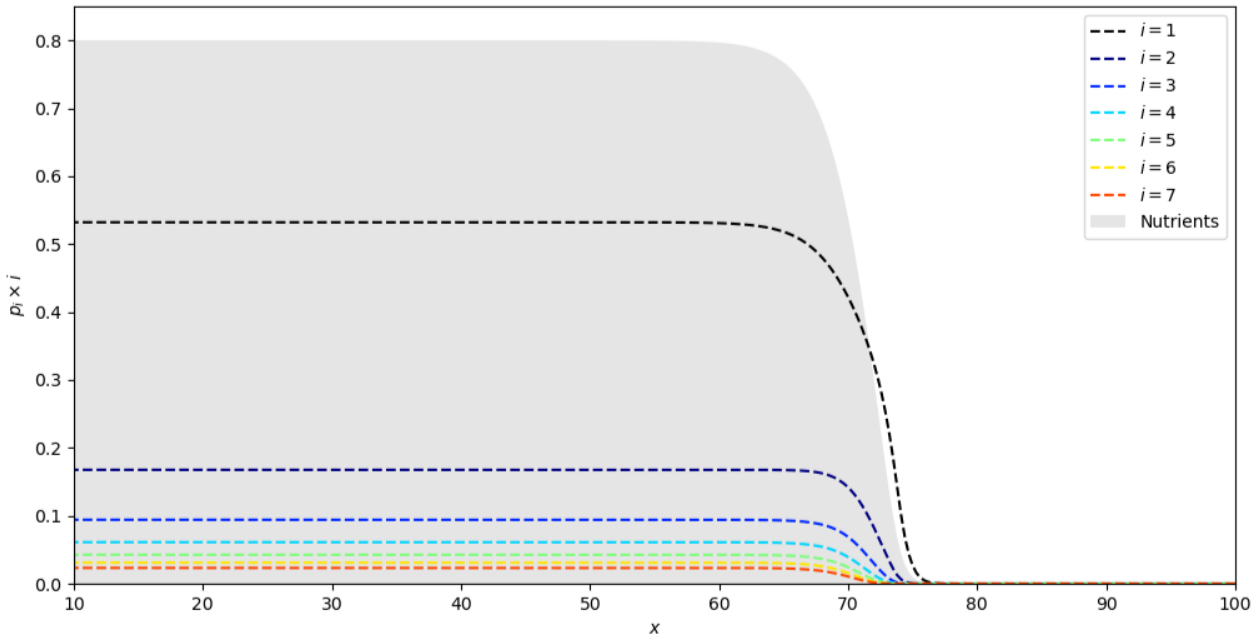

Figure 5: **Example of traveling wave solutions of the model** (4)-(5)-(6) **at time** $t = T$**.** The nutrient density, N, is represented in grey. The dashed lines correspond to the densities of different sizes of bacterial clusters multiplied by their size, $p_i(x) \times i$ at time $t = T$. The black line represents isolated bacteria, while the lines from blue to red correspond to bacterial clusters and more precisely, from the cluster of two bacteria in blue to the cluster of n bacteria in red. We observe an invasion of isolated bacteria, leading to the creation of nutrients. In the region where nutrients are present, we see the successive invasion of clusters of increasingly larger sizes. This spatial heterogeneity in the distribution of different cluster sizes has been recently observed biologically in the article [47]. The parameter values are given by $\beta = \gamma = \epsilon = \delta = \alpha_1 = \alpha_2 = N_M = 1$, $n = 10$, and the functions are defined as follows: $v(i) = \tau(i) = 1$ for all $i \in \{2, \dots, n\}$.

section, we adapt our model to the specific case of the $A+S-$ and $A-S+$ strains.

To model the $A+S-$ strain, we remove the transport term for bacterial clusters from the previous model, *i.e.* $v(i) = 0$ for all $i \in \{2, \dots n\}$. Similarly, for the $A-S+$ strain, we remove the transport term of isolated bacteria.

In Figure 6, we carry out numerical simulations similar to the biological experiments performed in the article [12]. Specifically, we carry out three independent numerical simulations, one for each strain, which we stop at the same time to compare the invasion of the three strains. The black curve corresponds to the *Wildtype* strain, the red curve to the $A+S-$ strain, and the green curve to the $A-S+$ strain. Our numerical results are consistent with the findings of the biological experiments; the $A-S+$ strain is significantly slower in invading the *E. coli* prey compared to the other strains.

For these parameter values, the invasion speed of the *Wildtype* strain is similar to the invasion speed of the $A+S-$ strain. However, as explained earlier, for other parameter values, the front can be pushed, and in that case, the speed of the *Wildtype* strain would be greater than the speed of the $A+S-$ strain. Regarding the biological experiments performed in the article [12], the $A+S-$ strain is slightly faster in terms of predation than the *Wildtype* strain. Nevertheless, these results are highly variable, and more experiments are needed to conclude a significant difference between these two strains. Note that, in the absence of prey, the *Wildtype* strain propagates significantly faster than both the $A+S-$ and $A-S+$ strains, demonstrating that motilities A and S are used synergistically [60]

2.3.3 Optimal motility strategy for invasion

The interest of the coexistence of the two motility systems is an important question in this field. As explained earlier, these two distinct motility systems lead to significant differences in bacterial movement characteristics. We assume that, for the reasons specified before, the diffusion coefficient remains unchanged for different cluster sizes, and only differences in instantaneous speed and persistence need to be considered. The A motility of isolated bacteria induces a relatively low speed but, in return, a very high persistence in the same direction. In contrast, the social motility of clusters generates a higher speed along one direction but a much lower persistence. To study the impact of these differences on predation speed, we examine the critical

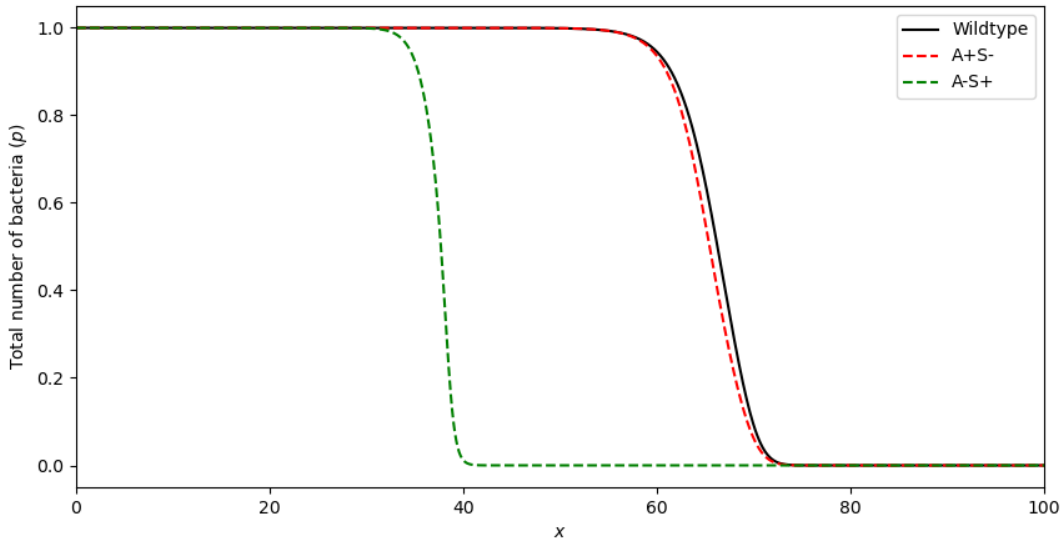

Figure 6: **Comparison of the invasion of the three different strains: *Wildtype*, $A+S-$, $A-S+$ at time $t = T$.** The black curve is a numerical solution of the model (4)-(5)-(6) associated with the *Wildtype* strain. The red (respectively green) curve is a numerical solution of the same model but without transport terms for clusters of bacteria (respectively for isolated bacteria) and corresponds to the $A+S-$ strain (respectively $A-S+$ strain). For the *Wildtype* strain and the $A+S-$ strain, the functions v and τ are defined as $v(i) = 1.25$ and $\tau(i) = 1/(1.25^2)$ for all $i \in \{2, \dots, n\}$. For the $A-S+$ strain, the functions v and τ are defined as $v(i) = 0$ and $\tau(i) = 1/(1.25^2)$ for all $i \in \{2, \dots, n\}$. The parameter values are: $n = 10$, $\beta = \gamma = \delta = \alpha_1 = \alpha_2 = N_M = 1$, $\epsilon = 0.5$.

speed of the model (4)-(5)-(6) for different couples of functions (v_j, τ_j) under the constraint $v_j^2 \tau_j = 1$, corresponding to the assumption that the diffusion coefficient D is equal to 1 for all cluster sizes (see (3)).

Several choices of function families are possible for instantaneous speed/persistence. We particularly study linear functions and Hill functions. First, we assume that the functions v_j are linear. More precisely, we assume that the family of functions $(v_j)_j$ corresponds to the lines connecting the point $(1, 1)$ to the point $(n, \bar{v}_{n,j})$, with $\bar{v}_{n,j} \in \mathbb{R}_+^\star$ corresponding to the speed of clusters of size n. When $\bar{v}_{n,j} < 1$, we have $v_j' < 0$, so the clusters are slower than isolated bacteria but, in return, will have a greater persistence ($\tau_j = 1/v_j^2$). We have the opposite result for $\bar{v}_j > 1$. Moreover, as $\bar{v}_j$ increases compared to 1, the difference in motility between isolated bacteria and clusters becomes more significant. In the top of Figure 7, we illustrate the family of functions $(v_j)_j$ (on the left) for different values of $(\bar{v}_j)_j$, as well as the associated family of functions, $(\tau_j)_j$ (on the right). In the bottom of Figure 7, we also plot the critical speed of the model (4)-(5)-(6), for the different couples of functions (v_j, τ_j) as a function of the coefficients $\bar{v}_j$ associated with these couples. The colors of the squares correspond to the color curves of the associated functions v_j and τ_j in the figures above. In Figure 8, we follow the same reasoning, but this time taking functions v_j in the form of Hill functions.

For both Figures 7 and 8, the results on the critical speed are similar. When the difference in instantaneous speed between clusters and isolated bacteria is either a disadvantage or too small an advantage, this difference in instantaneous speed/persistence does not affect the predation speed of bacteria *M. xanthus*. More specifically, in this case, the front is pulled. Indeed, the invasion speed is equal to the linear speed, which, for these parameter values, is the parabolic speed. However, when the speed advantage of bacterial clusters (coupled with the disadvantage of cluster persistence) becomes significant enough, the coexistence of A and S motility enables faster invasion of the prey. In this case, the front is pushed, and the impact on the predation speed is proportional to the difference in instantaneous speed/persistence. In other words, the coexistence of two motility systems either does not affect predation speed, and in this case, the invasion speed is solely influenced by isolated bacteria (pulled front), or it allows faster predation (pushed front). Thus, according to our model, the coexistence of two motility systems is never a disadvantage for predation.

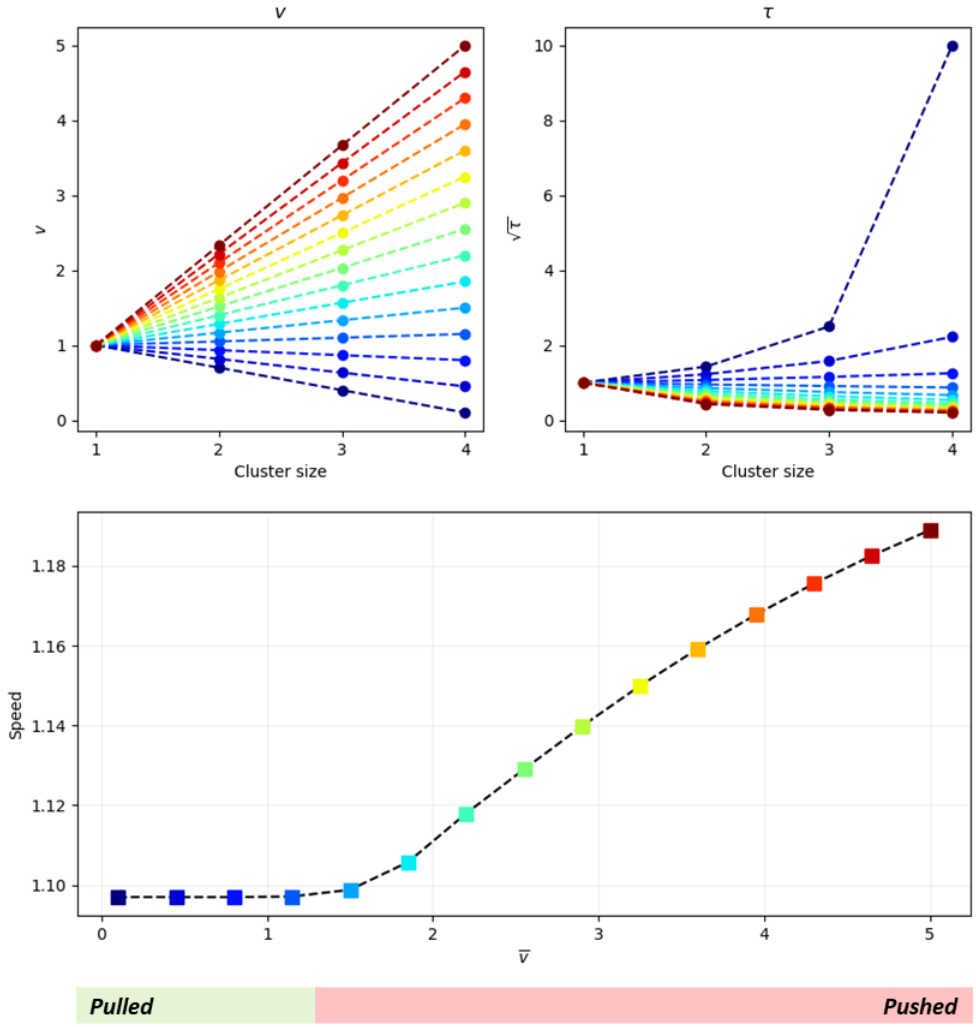

Figure 7: **Evolution of the numerical critical speed of the model** (4)-(5)-(6) **under the constraint** $1 = \tau v^2$ **with** v **a linear function. Top.** On the left, we represent a family of instantaneous speed functions v_j. The instantaneous speeds v_j are lines connecting the point $(1, 1)$ to the point $(n, \bar{v}_j)$, with $(\bar{v}_j)$ a uniform discretization of the interval $[0.1, 5]$, represented by the color spectrum from blue ($\bar{v} = 0.1$) to red ($\bar{v} = 5$). On the right, the figure illustrates the functions τ_j associated with instantaneous speeds v_j under the constraint $1 = v_j^2 \tau_j$. **Bottom.** For each couple of functions (v_j, τ_j), we numerically compute the critical speed of the model (4)-(5)-(6) and we indicate the result by a square with the corresponding colour. When $\bar{v}$ is small enough, the critical speeds are equal to the linear speed, and the front is pulled. In this case, the propagation speed is independent of the coefficient $\bar{v}$. However, when the coefficient, $\bar{v}$, becomes large enough, the front becomes pushed and predation of the bacteria is faster. The values of the other parameters are given by $n = 4$, $\epsilon = 0.9$, $\alpha_1 = \alpha_2 = \gamma = \beta = N_M = 1$ and $\delta = 3$.

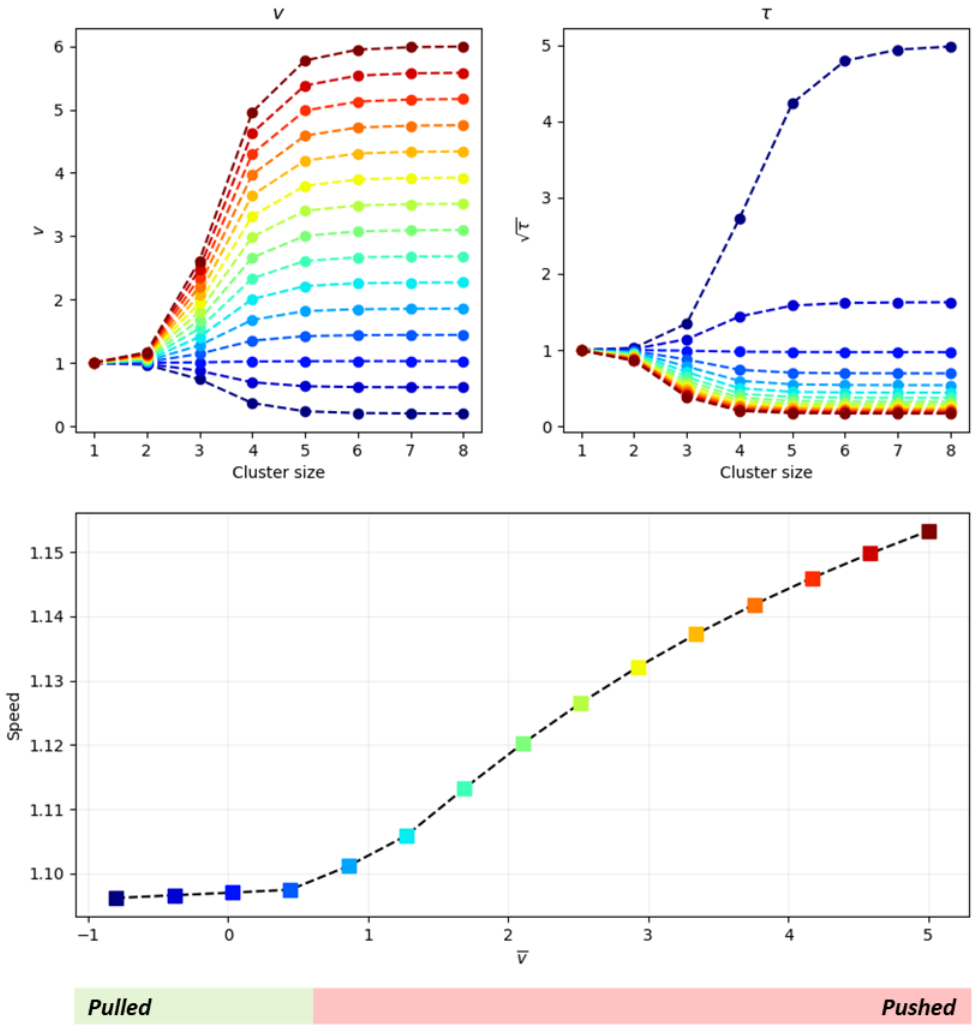

Figure 8: **Evolution of the numerical critical speed of the model** (4)-(5)-(6) **under the constraint** $1 = \tau v^2$ **with** v **a Hill function. Top.** On the left, we represent a family of instantaneous speed functions v_j. The functions v_j are of the form $v_j(i) = 1 + \bar{v}_j \cdot h(i)^m/(1 + h(i)^m)$, where h is an affine function given by $h(i) = i \cdot h_1 + h_0$, m is an integer and $(\bar{v}_j)$ a uniform discretization of the interval $[-1, 5]$. On the right, the figure illustrates the functions τ_j associated with instantaneous speeds v_j under the constraint $1 = v_j^2 \tau_j$. **Bottom.** For each couple of functions (v_j, τ_j), we numerically compute the critical speed of the model (4)-(5)-(6) and we indicate the result by a square with the corresponding colour. When $\bar{v}$ is small enough, the critical speeds are equal to the linear speed, and the front is pulled. In this case, the propagation speed is independent of the coefficient $\bar{v}$. However, when the coefficient, $\bar{v}$, becomes large enough, the front becomes pushed and predation of the bacteria is faster. The values of the other parameters are given by $n = 8$, $\epsilon = 0.9$, $\alpha_1 = \alpha_2 = \gamma = \beta = N_M = 1$, $\delta = 3$, $m = 10$, $h_0 \approx 0.28$ and $h_1 \approx 0.21$.

3 Conclusion

In this work, we introduce a model concerning the predation of the social bacterium *Myxococcus xanthus*. This model, corresponding to an extension of previous models, aims primarily to model and study the impact of differences between the two motility systems, A and S. For this model, we determine a formula for the linear speed. Particularly, we demonstrate the presence of anomalous speeds caused by the linear coupling between the clusters and the isolated bacteria. Regarding the speed of the nonlinear model, our numerical simulations show the existence of a transition between the pulled-front regime and the pushed-front regime, in which the selected speed exceeds the linear prediction.

From a modelling point of view, the numerical simulations of our model verify characteristics presented in biological experiments. Specifically, our model confirms the spatial distribution of different cluster sizes in the invasion front. It also provides an explanation for biological experiments on the invasion speed of the *Wildtype*, $A+S-$, and $A-S+$ strains. As the experiments showed, the $A-S+$ strain had great difficulty in invading the prey. Furthermore, we use our model to show that the coexistence of the two motility systems, A and S, has either a neutral or a positive effect on faster predation. If the difference in motility does not lead to sufficiently large differences in instantaneous speed and persistence, this coexistence will not influence the propagation speed. Conversely, if this difference is significant enough, it will proportionally induce an increase in the invasion speed.

To determine whether the coexistence of A and S motility has a neutral or positive impact on predation, it is crucial to determine precisely the transition between a pulled-front and a pushed-front regime. However, numerically approximating this transition with high precision is complex. A new numerical method, based on far-field decomposition, makes it possible to approximate this transition with extreme accuracy for a large family of reaction-diffusion systems [61]. It would be interesting to extend these results to hyperbolic systems. Once this threshold has been precisely calculated, it would be interesting to determine biologically reasonable parameter values in order to determine the associated front regime: pulled or pushed.

In comparison to other bacterial predators specialized in specific prey, *Myxococcus xanthus* stands out as a generalist predator capable of feeding on a wide variety of prey [9]. Due to the

vast spectrum of potential prey for *Myxococcus xanthus*, the predation process of this bacterium is likely to be extremely complex, involving various molecular mechanisms acting independently or synergistically to attack different species. It would therefore be relevant to explore, both mathematically and biologically, the variations in the predation process exerted by *M. xanthus* on different prey species. Additionally, some bacterial prey, such as *Bacillus subtilis*, *Pseudomonas fluorescens* and *Escherichia coli*, adopt defensive strategies, including the formation of specific biofilms or the secretion of antibiotics [62, 63, 64, 65]. Therefore, it could also be interesting to study the defensive reactions of prey against the predator.

In this article, we focused on the predation front of *M. xanthus*. In the wake of the invasion front, two main phenomena occur successively: *rippling* and then the formation of fruiting bodies. Following the advance of the predation front, the presence of cellular debris allows *M. xanthus* cells to coordinate their movement by forming accordion-like undulations, similar to the undulations of water [8, 66, 67, 68, 69]. During these undulations, called *ripples*, each wave crest oscillates back and forth without generating a net displacement, although individual cells change their positions. Then, in times of starvation, cells form aggregates, exchanging extracellular chemical signals as well as signals from physical contact, thereby creating multicellular fruiting bodies [70]. The cells involved in fruiting bodies undergo transformation into myxospores, highly resistant to heat [71]. Sporulation has the advantage of enabling survival in hostile environments and increasing germination and growth rates when the cells encounter favourable conditions.

In the literature, there are already several models of different natures aimed at modelling rippling [69, 72, 73], including models with *Run and Tumble* motion [27, 74, 30]. Similarly, numerous models have been introduced to model the formation of fruiting bodies (see, for example, [75, 76, 77]). In order to develop a model encompassing all these phenomena, it would be interesting to extend our hyperbolic model to determine if it can also describe, in the wake of the invasion front, the rippling phenomenon and then, once nutrients are depleted, the formation of fruiting bodies. The existence of periodic solutions in space (formation of fruiting bodies) and/or in time (rippling) are phenomena that have already been extensively studied for hyperbolic equations and systems of equations [78, 79, 80, 81, 82, 83, 84].

Acknowledgement

The author was funded by the ANR via the project PLUME under grant agreement ANR-21-CE13-0040. The author thanks Vincent Calvez for several insightful discussions. In addition, the author gratefully acknowledges Antoine Le Gall and Tâm Mignot for their helpful explanations regarding the bacterium Myxococcus xanthus. This project has received funding from the European Research Council (ERC) under the European Union's Horizon 2020 research and innovation programme (grant agreement No 865711).

A Derivation of the linear propagation speed for $n = 2$

First, we provide the definition of the term *pinched double roots* from [49, Defintion 4.2]

Definition 2 (Pinched double root)**.** *We say* $(\nu_\star, \lambda_\star)$ *is a* pinched double root *of the dispersion relation* $D_s(\nu, \lambda)$ *if*

1. Double root: *we have*

$$D_s(\nu_\star, \lambda_\star) = 0, \quad \textit{and}, \quad \partial_\nu D_s(\nu_\star, \lambda_\star) = 0. \tag{A.1}$$

2. Pinching: *there exists a continuous curve* $\lambda(\tau)$*, with* $\tau \in \mathbb{R}_+$ *satisfying:*

   - $\mathrm{Re}\ \lambda(\tau)$ *is strictly increasing,*
   - $\lambda(0) = \lambda_\star$*,*
   - *and* $\mathrm{Re}\ \lambda(\tau) \to \infty$ *as* $\tau \to \infty$*,*

   and continuous curves of roots $\nu^\pm(\lambda(\tau))$ *which satisfy*

   - $\nu^\pm(\lambda_\star) = \nu_\star$*,*
   - *and*

$$\lim_{\tau \to \infty} \mathrm{Re}\ \nu^\pm(\lambda(\tau)) = \pm\infty. \tag{A.2}$$

In this work, we are only interested in time-stationary fronts in the moving frame reference. Consequently, we consider the values $\lambda \in \mathbb{R}^+$, and negative eigenvalues, $\nu \in \mathbb{R}^-$.

Derivation of *normal* speeds. In the decoupled case, $k = 0$, the first two equations (9a)-(9b) give us the following system

$$\begin{cases} \partial_t p_1^+ + \dfrac{1}{\epsilon}\partial_x p_1^+ = \dfrac{1}{2\epsilon^2}(p_1^- - p_1^+) + \dfrac{\alpha_1}{2}p_1, & \text{(A.3a)} \\ \partial_t p_1^- - \dfrac{1}{\epsilon}\partial_x p_1^- = \dfrac{1}{2\epsilon^2}(p_1^+ - p_1^-) + \dfrac{\alpha_1}{2}p_1, & \text{(A.3b)} \end{cases}$$

which can be expressed as,

$$\epsilon^2\partial_{tt}p_1 + (1 - \alpha_1\epsilon^2)\partial_t p_1 = \partial_{xx}p_1 + \alpha_1 p_1.$$

This linear equation has been extensively studied (See for example [36, 42]). In particular, it has been shown that the associated critical propagation speed is given by the following formula

$$\begin{cases} \dfrac{2\sqrt{\alpha_1}}{1+\epsilon^2\alpha_1}, & \text{if } \epsilon \leq 1/\sqrt{\alpha_1}, \qquad \text{(Parabolic regime)} \\ \dfrac{1}{\epsilon}, & \text{otherwise.} \qquad \text{(Hyperbolic regime)} \end{cases} \tag{A.4}$$

In the parabolic regime, the speed is a perturbation of the critical speed of the Fisher-KPP parabolic equation. While, for the hyperbolic regime, the critical speed corresponds to the maximum possible speed of the wave, which is equal to the coefficient of the transport term.

In the moving frame, $\xi = x - st$, we seek solutions in the exponential form $e^{\lambda t + \nu\xi}\overline{p_1}$, we obtain the following dispersion relation,

$$D_s^{(1)}(\nu, \lambda) = \nu^2 + \nu\frac{s}{1-\epsilon^2 s^2}(1 - \alpha_1\epsilon^2 - 2\lambda\epsilon^2) + \frac{1}{1-\epsilon^2 s^2}\left[\alpha_1 - \epsilon^2\lambda^2 - (1-\alpha_1\epsilon^2)\right],$$

with the two following associated roots,

$$\nu_1^{\pm}(\lambda, s; \alpha_1, \epsilon) = \frac{s(1-\alpha_1\epsilon^2) + 2s\epsilon^2\lambda \mp \sqrt{s^2(1+\alpha_1\epsilon^2)^2 - 4\alpha_1 + 4\lambda(1-\alpha_1\epsilon^2+\lambda\epsilon^2)}}{2(\epsilon^2 s^2 - 1)}. \tag{A.5}$$

The dispersion relation has a double root when $\nu_1^+ = \nu_1^-$. Since the speed of $p_1^{\pm}$ is given by the value $1/\epsilon$, we consider only the range of plausible invasion speeds $s \in]0, 1/\epsilon]$. By performing a Taylor expansion of the eigenvalues as $\lambda \to \infty$, we obtain the following relation

$$\nu_1^{\pm}(\lambda, s) = \frac{\lambda\epsilon}{(\epsilon s \pm 1)} + \underset{\lambda\to+\infty}{o}(\lambda).$$

Consequently, we have the following limit, $\nu_1^{\pm}(\lambda, s) \to \pm\infty$ as $\lambda \to +\infty$. The pinching condition is therefore satisfied. The equality $\nu_1^+ = \nu_1^-$ gives us

$$s_1^2(\lambda; \alpha_1, \epsilon) = \frac{4\alpha_1}{(1+\alpha_1\epsilon^2)^2} - \frac{4\lambda(1-\alpha_1\epsilon^2+\lambda\epsilon^2)}{(1+\alpha_1\epsilon^2)^2}. \tag{A.6}$$

To determine the linear propagation speed, we need to minimize the function Λ defined by

$$\Lambda(\lambda; \alpha_1, \epsilon) := \frac{4\lambda(1 - \alpha_1\epsilon^2 + \lambda\epsilon^2)}{(1 + \alpha_1\epsilon^2)^2}.$$

- When $\epsilon \leq 1/\sqrt{\alpha_1}$, the minimum of the function Λ is reached at $\lambda = 0$. In this case, we indeed obtain the parabolic propagation speed.

$$s_1 = s_{\text{para}} := \frac{2\sqrt{\alpha_1}}{1 + \epsilon^2\alpha_1},$$

  already demonstrated by Hadeler [36] and Fedotov [38] using completely different methods.

- When $\epsilon > 1/\sqrt{\alpha_1}$, the minimum of the function Λ is reached at $\lambda = \lambda^\star$, with $\lambda^\star := -(1 - \alpha_1\epsilon^2)/(2\epsilon^2)$. Substituting this into equation (A.6), we obtain the hyperbolic propagation speed $s_1 = s_{\text{hyp}} := 1/\epsilon$. In this case, the associated $\nu^\star$ is null. Contrary to the pinched double root of the parabolic case, the one of the hyperbolic case is not simple relatively to λ.

Consequently, the concept of pinched double roots allows us to easily obtain the critical linear speed of the system (A.3a)-(A.3b), which was already demonstrated in the article [42] using a different method.

Derivation of *anomalous* speeds. To determine a potential anomalous speed, we now consider equations (9c)-(9d). Following a similar approach as in the previous analysis, we can derive the pair of eigenvalues associated with the system of two equations (9c)-(9d). These eigenvalues, denoted as ν_2^- and ν_2^+, are defined by

$$\nu_2^\pm(\lambda, s; \epsilon, v, \tau, k) = \frac{s(1 + 2\epsilon^2\tau k) + 2\epsilon^2\tau\lambda s \mp \sqrt{4\lambda\tau v^2\left(1 + 2\epsilon^2\tau k + \epsilon^2\tau\lambda\right) + s^2 + 4k\tau v^2(1 + \epsilon^2\tau k)}}{2\tau(\epsilon^2 s^2 - v^2)}. \tag{A.7}$$

The dispersion relation for the complete linear system (9a)-(9d), due to the triangular structure of the problem, is given by the following formula:

$$D_s(\nu, \lambda) := \left(\nu - \nu_1^+(\lambda, s)\right)\left(\nu - \nu_1^-(\lambda, s)\right)\left(\nu - \nu_2^+(\lambda, s)\right)\left(\nu - \nu_2^-(\lambda, s)\right).$$

This dispersion relation has double roots if one of the equalities $\nu_1^+ = \nu_1^-$, $\nu_2^+ = \nu_2^-$, $\nu_1^+ = \nu_2^-$ and $\nu_1^- = \nu_2^+$ is satisfied. As previously shown, the double root when $\nu_1^+ = \nu_1^-$ is pinched and

leads to parabolic and hyperbolic speeds. The equality $\nu_2^+ = \nu_2^-$ is associated with a complex propagation speed. Let us now consider the equality $\nu_1^- = \nu_2^+$. When ν_2^+ is real, its sign is always positive according to definition (A.7). Therefore, we do not consider this equality. Finally, we examine the last double root $\nu_1^+ = \nu_2^-$. This time, analyzing the signs of the eigenvalues shows that consistent triplets (ν, s, λ) can be obtained. As we have seen before, ν_1^+ tends to $+\infty$ as $\lambda \to +\infty$. Conversely, the expansion of ν_2^- for $\lambda \to +\infty$ is given by the following relation

$$\nu_2^-(\lambda, s) = \frac{\lambda\epsilon}{\epsilon s - v} + \underset{\lambda\to+\infty}{o}(\lambda).$$

Consequently, when $s < v/\epsilon$, we have the limit $\nu_2^- \to -\infty$ as $\lambda \to +\infty$. Here, the possible wave propagation speeds, s, lie between 0 and $\max(1/\epsilon, v/\epsilon)$. Therefore, it is possible to have $s > v/\epsilon$ when $v < 1$. In this case, the root does not satisfy the pinching condition, and no anomalous speed is expected.

The anomalous speed associated with the equality $\nu_1^+ = \nu_2^-$ is a solution of the following polynomial equation,

$$a_4 s^4 + a_2(\lambda) s^2 + a_0(\lambda) = 0, \tag{A.8}$$

with

$$a_0(\lambda) := \left((\lambda + k)\left[1 + \epsilon^2\tau(\lambda + k)\right] - \tau v^2(\lambda - \alpha_1)\left[1 + \epsilon^2\lambda\right]\right)^2, \tag{A.9}$$

$$\begin{aligned} a_2(\lambda) := \big[&(1 - \alpha_1\epsilon^2)(1 + 2\epsilon^2\tau k) + 2\alpha_1\tau\epsilon^2 - 2k\epsilon^2(1 + \epsilon^2\tau k)\big] \\ &\left\{(\lambda + k)\left[1 + \epsilon^2\tau(\lambda + k)\right] + \tau v^2(\lambda - \alpha_1)\left[1 + \epsilon^2\lambda\right]\right\} \\ &- \tau v^2(1 + \alpha_1\epsilon^2)^2(\lambda + k)\left[1 + \epsilon^2\tau(\lambda + k)\right] - (\lambda - \alpha_1)(1 + \lambda\epsilon^2), \end{aligned} \tag{A.10}$$

and,

$$a_4 := \epsilon^2(\alpha_1 + k)(k\epsilon^2 - 1)(\tau[k\epsilon^2 - 1] + 1)(1 + \epsilon^2 k\tau + \alpha_1\epsilon^2\tau). \tag{A.11}$$

Solving equation (A.8) gives us two possibles real positive speeds

$$s^{\pm}(\lambda) := \sqrt{\frac{-a_2(\lambda) \pm \sqrt{a_2^2(\lambda) - 4a_0(\lambda)a_4}}{2a_4}}. \tag{A.12}$$

We define $\Gamma^{\pm}$ as the sets given by

$$\Gamma^{\pm} = \{\lambda \in \mathbb{R}^+ :\ \nu(\lambda, s^{\pm}(\lambda)) \text{ is a pinched double root of } D_s \text{ associated with admissible } (s^{\pm}, \nu)\}.$$

Conjecture 1. *If* $\Gamma^+ \cup \Gamma^- \neq \varnothing$*, then* $0 \in \Gamma^+ \cup \Gamma^-$*, and we have the following results:*

- *If* $0 \in \Gamma^+$*, then*

$$s^+(0) \geq \max\left(\max_{\lambda\in\Gamma^+} s^+(\lambda), \max_{\lambda\in\Gamma^-} s^-(\lambda)\right).$$

- *If* $0 \in \Gamma^-$*, then*

$$s^-(0) \geq \max\left(\max_{\lambda\in\Gamma^+} s^+(\lambda), \max_{\lambda\in\Gamma^-} s^-(\lambda)\right).$$

In other words, when there exists a family of admissible pinched double roots associated with the equality $\nu_1^+ = \nu_2^-$ *parameterized by* λ*, the maximum associated speed is given by the one at* $\lambda = 0$*.*

The high complexity of the polynomial coefficients (A.9), (A.10), and (A.11) makes proving such a result challenging. To ensure its validity, we verified that this result holds true for 10^{15} different parameter values, uniformly distributed in the parameter space $(\alpha_1, \epsilon, \tau, v, k) \in [0.05, 10]^5$. For each of these tests, the maximum admissible speed was indeed located at $\lambda = 0$.

Under the assumption of the conjecture 1, we thus define the two anomalous speeds of our problem given by

$$s^{\pm}_{\text{anom}} := s^{\pm}(0) = \sqrt{\frac{-a_2(0) \pm \sqrt{a_2^2(0) - 4a_0(0)a_4}}{2a_4}}. \tag{A.13}$$

Unlike speeds for the parabolic and hyperbolic regimes, these anomalous speeds depend on the parameters v, τ, and k. When $\epsilon = 0$, the term a_4 becomes zero, thus there is only one anomalous speed, which is given by the formula,

$$s^{\pm}_{\text{anom}}(\epsilon = 0) = \alpha_1 \frac{\sqrt{\theta - 1}}{\sqrt{k + \alpha_1}} + \frac{\sqrt{\alpha_1 + k}}{\sqrt{\theta - 1}},$$

with $\theta = \tau v^2$. This equality is in good agreement with the result obtained in the article [51].

To conclude, we obtain the following result:

Proposition 1 (Linear propagation speed for $n = 2$)**.** *We assume conjecture 1. By definition 1, the critical linear propagation speed,* $s^\star_{lin}$*, can take one of four possible values:*

- *The two normal speeds: parabolic and hyperbolic*

$$s_{para} := \frac{2\sqrt{\alpha_1}}{1 + \alpha_1\epsilon^2}, \qquad s_{hyp} := \frac{1}{\epsilon}.$$

- *The two anomalous speeds:*

$$s^{\pm}_{anom} = s^{\pm}(0) = \sqrt{\frac{-a_2(0) \pm \sqrt{a_2^2(0) - 4a_0(0)a_4}}{2a_4}},$$

with a_0*,* a_2*, and* a_4 *defined by equations* (A.9)*,* (A.10)*, and* (A.11)*, respectively.*

Numerical simulations. In this section, we focus on the selected wave speed for a nonlinear model sharing the same linear part of the model (8). More precisely, we introduce a nonlinear model without certain nonlinear terms such as coagulation, in order to have fronts always linearly determined. This allows us to numerically verify whether the linear speed predicted by Proposition 1 is indeed the one selected by a nonlinear model in the pulled front regime.

We consider the following nonlinear model,

$$\begin{cases} \partial_t p_1^+ + \dfrac{1}{\epsilon}\partial_x p_1^+ = \dfrac{1}{2\epsilon^2}(p_1^- - p_1^+) + \dfrac{k}{2}p_2(1-p_1) + \dfrac{\alpha_1}{2}p_1(1-p_1), & \text{(A.14a)} \\ \partial_t p_1^- - \dfrac{1}{\epsilon}\partial_x p_1^- = \dfrac{1}{2\epsilon^2}(p_1^+ - p_1^-) + \dfrac{k}{2}p_2(1-p_1) + \dfrac{\alpha_1}{2}p_1(1-p_1), & \text{(A.14b)} \\ \partial_t p_2^+ + \dfrac{v}{\epsilon}\partial_x p_2^+ = \dfrac{1}{2\tau\epsilon^2}(p_2^- - p_2^+) - kp_2^+, & \text{(A.14c)} \\ \partial_t p_2^- - \dfrac{v}{\epsilon}\partial_x p_2^- = \dfrac{1}{2\tau\epsilon^2}(p_2^+ - p_2^-) - kp_2^-. & \text{(A.14d)} \end{cases}$$

corresponding to an hyperbolic extension of the model presented in the article [51].

In Figure A.1, we plot the selected speed of the model (A.14a)-(A.14d) using numerical simulations (black points) and the theoretical linear speeds presented in Proposition 1 (colored lines) for various values of the parameter ϵ. We observe that the numerical selected speed indeed corresponds to the predicted linear speed. When ϵ is small enough, the linear speed matches the parabolic speed (red line). As ϵ increases, the selected speed first becomes the *minus* anomalous speed (cyan line) and then the *plus* anomalous speed (magenta line). For other simulations not presented in this article, with different parameter values, we have also observed the possibility to select the hyperbolic speed (green line).

For the parabolic and anomalous regimes, the linear propagation speed is determined by a simple pinched double root at $\lambda = 0$. In these regimes, our numerical simulations show that the modified nonlinear model indeed selects the marginally stable front. For these initial steep conditions, this scenario is expected and corresponds to the *marginal stability conjecture*. (see [85, 86, 87, 49] for further details). This conjecture was recently proven in the context of higher-order

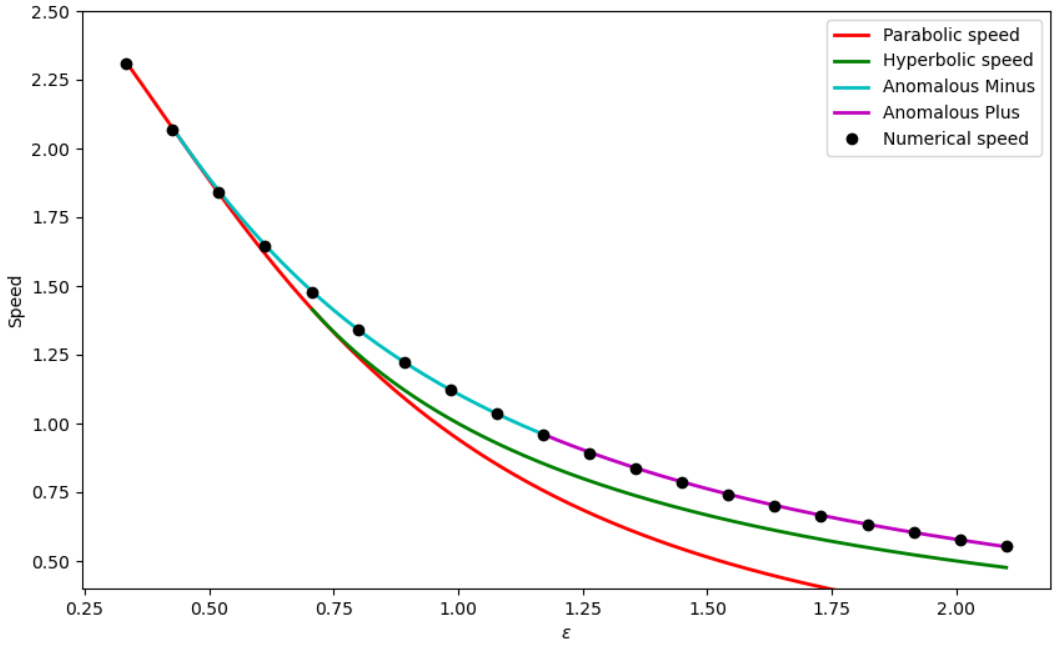

Figure A.1: **Comparison between the numerical selected speed of the modified model** (A.14a)-(A.14d) **and various linear speeds for different values of ϵ.** The numerical selected speed of the model (A.14a)-(A.14d) is represented by black points. The theoretical linear speeds are depicted by solid colored lines: red (*parabolic*), green (*hyperbolic*), cyan/magenta (*anomalous minus/plus*). The selected speed of the model (A.14a)-(A.14d) aligns with the linear prediction of Proposition 1. The parameter values are given by: $k = 2$, $\alpha_1 = 2$, $v = 1.5$, $\tau = 1$.

scalar parabolic equations by Avery and Scheel in [88], and later extended to reaction-diffusion systems by Avery [89].

For the hyperbolic regime, the linear propagation speed is induced by a double pinched double root at $\lambda = \lambda^\star > 0$. This type of situation is more complex and has been studied, for instance, in the articles [49, 90, 91]. In this situation, it is possible to overestimate pointwise growth rates and fail to correctly determine the marginally stable front [49, Remark 4.5]. According to our numerical simulations, we observe that this speed can indeed be selected by the model (A.14a)-(A.14d). For example, under the assumption $v < 1$ and $\epsilon > 1/\sqrt{\alpha_1}$, the hyperbolic speed is always selected.

B Derivation of the linear propagation speed for $n > 2$

Linear propagation speed. Linearizing around the zero equilibrium point, we obtain the following linear system

$$\begin{cases} \partial_t p_1^{\pm} \pm \dfrac{1}{\epsilon}\partial_x p_1^{\pm} = \pm\dfrac{1}{2\epsilon^2}(p_1^- - p_1^+) + \displaystyle\sum_{j=2}^{n} \beta(j)\eta(j,1)p_j + \frac{\alpha_1}{2}p_1, \\ \partial_t p_i^{\pm} \pm \dfrac{v(i)}{\epsilon}\partial_x p_i^{\pm} = \pm\dfrac{1}{2\tau(i)\epsilon^2}(p_i^- - p_i^+) + \displaystyle\sum_{j=i+1}^{n} \beta(j)\eta(j,i)p_j - \beta(i)p_i^{\pm}, \quad \text{for all } i \in \{2,\dots,n\}. \end{cases} \tag{B.1}$$

The derivation of the linear propagation speed is similar to the case $n = 2$. Due to the triangular structure of the system (B.1), the dispersion relation is given by

$$D_s(\nu,\lambda) = \prod_{i=1}^{n} \left(\nu - \nu_i^+(\lambda,s)\right)\left(\nu - \nu_i^-(\lambda,s)\right), \tag{B.2}$$

where $\nu_i^{\pm}$ corresponds to the pair of eigenvalues associated with the two equations for clusters of size i, independent of all the other equations, i.e., under the assumption $\beta(j) = 0$ for all $j > i$. Consequently, $\nu_1^{\pm}$ are the same as previously, explicitly defined by equations (A.5). The eigenvalues $\nu_i^{\pm}$, for all $i \in \{2,\dots,n\}$, are defined by equation (A.7) in the case $k = \beta(i)$, $v = v(i)$, and $\tau = \tau(i)$.

The pinched double roots of (B.2) associated with an admissible speed and slope can be obtained when $\nu_1^+ = \nu_1^-$ or when one of the equalities $\nu_1^+ = \nu_i^-$ with $i \in \{2,\dots,n\}$ is satisfied. In the first case, the associated speeds are the two normal speeds, while the second case leads to anomalous propagation speeds. For each cluster size $i \in \{2,\dots,n\}$, we assume the equivalent of conjecture 1, allowing us to define the two anomalous speeds for each cluster size.

$$s_{\text{anom},i}^{\pm} := s_i^{\pm}(0) = \sqrt{\frac{-a_{2,i}(0) \pm \sqrt{a_{2,i}^2(0) - 4a_{0,i}(0)a_{4,i}}}{2a_{4,i}}}, \quad \text{for } i \in \{2,\dots,n\}. \tag{B.3}$$

where the coefficients $a_{0,i}$, $a_{2,i}$, and $a_{4,i}$ are calculated in the same way as the coefficients a_0, a_2, and a_4, defined respectively by equations (A.9), (A.10), and (A.11).

We thus obtain the following proposition:

Proposition 2 (Critical linear propagation speed for $n > 2$)**.** *We assume conjecture 1 for the different cluster sizes. By definition 1, the critical linear propagation speed, $s_{lin}^{\star}$, can take the following possible values:*

- *The two normal speeds: parabolic and hyperbolic*

$$s_{para} := \frac{2\sqrt{\alpha_1}}{1+\alpha_1\epsilon^2}, \qquad s_{hyp} := \frac{1}{\epsilon}.$$

- *The different anomalous speeds:* $s^{\pm}_{anom,i}$ *for all* $i \in \{2,\dots,n\}$.

As before, the linear speed selected among these possible linear speeds corresponds to the maximum of the admissible speeds.

Numerical simulations. As previously, we introduce a nonlinear system that shares the same linear system (B.1), but whose nonlinear terms are chosen to have no impact on the wave speed,

$$\begin{cases} \partial_t p_1^{\pm} \pm \dfrac{1}{\epsilon}\partial_x p_1^{\pm} = \pm\dfrac{1}{2\epsilon^2}(p_1^- - p_1^+) + \displaystyle\sum_{j=2}^{n} \beta(j)\eta(j,1)p_j + \frac{\alpha_1}{2}p_1(1-p), \\ \partial_t p_i^{\pm} \pm \dfrac{v(i)}{\epsilon}\partial_x p_i^{\pm} = \pm\dfrac{1}{2\tau(i)\epsilon^2}(p_i^- - p_i^+) + \displaystyle\sum_{j=i+1}^{n} \beta(j)\eta(j,i)p_j - \beta(i)p_i^{\pm}, \quad \forall i \in \{2,\dots,n\}. \end{cases} \tag{B.4}$$

Case $n = 3$. In the first step, we assume that $n = 3$ to simplify the problem. There are six admissible linear speeds: the parabolic speed, the hyperbolic speed, the two anomalous speeds associated with clusters of size 2, and finally the two anomalous speeds associated with clusters of size 3.

In Figure B.1, we plot the selected speed of the modified model (B.4) using numerical simulations (black points), as well as the admissible theoretical normal and anomalous linear speeds (colored lines) for different parameter values of $v(3)$. The anomalous speed associated with clusters of size 2, $s^{\pm}_{\text{anom},2}$, is represented in blue while the anomalous speed associated with cluster of size 3, $s^{\pm}_{\text{anom},3}$, is in yellow. Again, for the numerical simulations, we consider only steep initial data. For this choice of parameter values, the hyperbolic speed is not admissible, and the only normal linear speed is the parabolic speed, represented by the red curve. To illustrate the phenomenon of anomalous speed selection, presented in Definition 1 and Proposition 2, we vary the value of $v(3)$ so that the admissible anomalous speed associated with clusters of three bacteria becomes greater than the admissible anomalous speed associated with clusters of two bacteria. As we can see in Figure B.1, the selected speed will transition from the anomalous speed associated with clusters of two bacteria to the anomalous speed associated with clusters of size three.

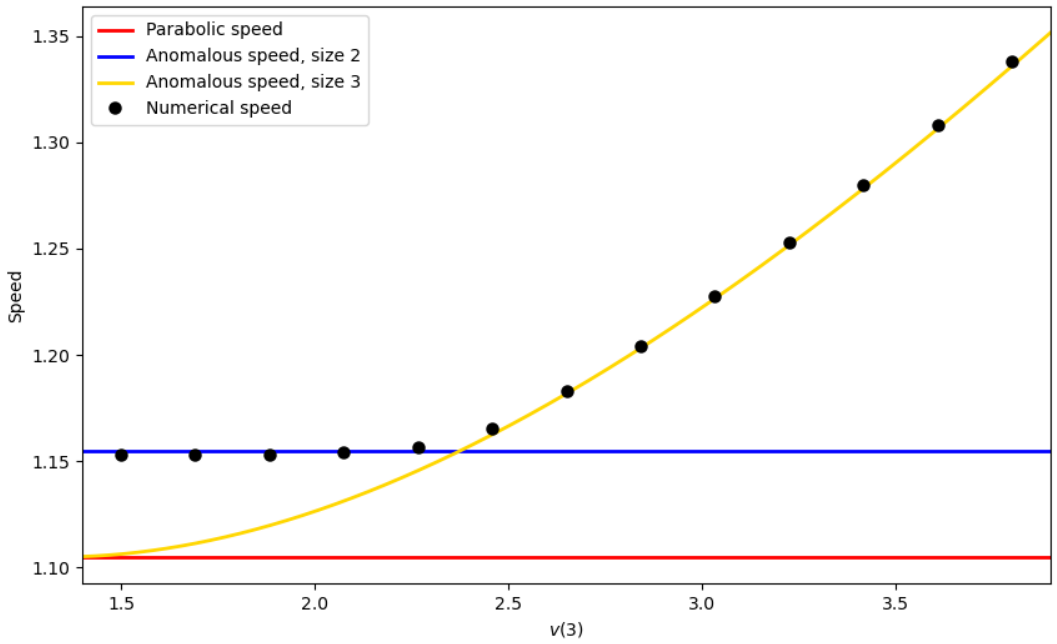

Figure B.1: **For $n = 3$, comparison between the numerical selected speed of the modified model** (B.4) **and various linear speeds for different values of** $v(3)$**.** The black dots correspond to the numerical selected speed of the system (B.4). The red curve represents the parabolic speed, the blue curve the anomalous speed associated with cluster of size 2, $s^{\pm}_{\text{anom},2}$, and finally, the yellow curve corresponds to the anomalous speed associated with cluster of size 3, $s^{\pm}_{\text{anom},3}$. For this parameter regime, the hyperbolic speed is not admissible. The parameter values are given by $\beta = 1$, $\alpha_1 = 1$, $\epsilon = 0.9$, and the functions τ and v are given by $\tau(2) = \tau(3) = 1$ and $v(2) = 2$.

Case $n > 3$. We also perform numerical simulations in the case $n > 3$. In Figure B.2, we plot the numerical selected speed of the modified model (B.4) using black dots, as well as the theoretical linear speeds for different values of the parameter ϵ and for two different cases, $n = 8$ and $n = 12$. When ϵ is small enough, the linear speed indeed corresponds to the parabolic speed, represented by the red curve. For both figures, the results are similar. When ϵ becomes large enough, the numerical speed becomes the largest of the admissible anomalous speeds represented by the blue curve. We also illustrate the hyperbolic speed with the green curve, even though it is never selected for these parameter values. These numerical results are in agreement with the Proposition 2.

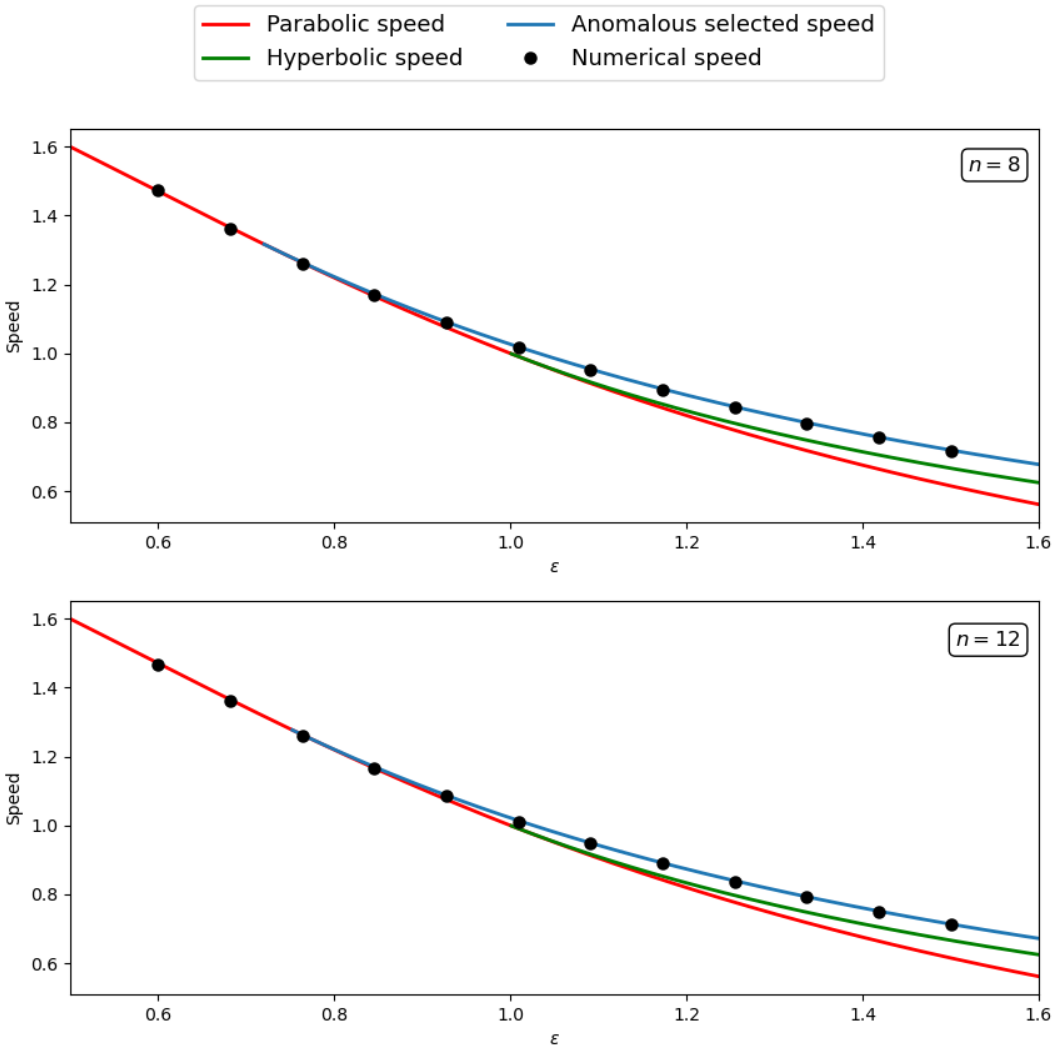

Figure B.2: **Comparison between the numerical selected speed of the modified model** (B.4) **and the various possible linear speeds for different values of ϵ, and for: Top, $n = 8$; Bottom, $n = 12$.** The black dots represent the numerical selected speed of the system (B.4). The red (resp. green) curve corresponds to the parabolic (resp. hyperbolic) linear speed. The largest of the admissible anomalous speeds is represented by the blue curve. The numerical simulations in the two figures are in agreement with Proposition 2. The values of the other parameters are $\beta = 1$, $\alpha_1 = 1$, and the functions τ and v are given by $\tau(i) = 1$ and (Top) $v(i) = 1 + 1.3 \times \mathbf{1}_{i\leq 4}(i)$, (Bottom) $v(i) = 1 + 1.6 \times \mathbf{1}_{i\leq 6}(i)$ for all $i \in \{2, \dots, n\}$.

References

[1] L. M. Faure et al. "The mechanism of force transmission at bacterial focal adhesion complexes". In: *Nature* 539.7630 (2016). DOI: 10.1038/nature20121.

[2] R. Mercier et al. "The polar Ras-like GTPase MglA activates type IV pilus via SgmX to enable twitching motility in *Myxococcus xanthus*". In: *Proceedings of the National Academy of Sciences* 117.45 (2020). DOI: 10.1073/pnas.2002783117.

[3] J. Hodgkin and D. Kaiser. "Genetics of gliding motility in Myxococcus xanthus (Myxobacterales): Two gene systems control movement". In: *Molecular and General Genetics MGG* 171.2 (1979). DOI: 10.1007/BF00270004.

[4] E. Rosenberg and M. Varon. "Antibiotics and Lytic Enzymes". In: *Myxobacteria*. Ed. by A. Rich and E. Rosenberg. Series Title: Springer Series in Molecular Biology. New York, NY: Springer New York, 1984. DOI: 10.1007/978-1-4613-8280-5_5.

[5] A. D. Morgan et al. "Comparative Analysis of *Myxococcus* Predation on Soil Bacteria". In: *Applied and Environmental Microbiology* 76.20 (2010). DOI: 10.1128/AEM.00414-10.

[6] J. Muñoz-Dorado et al. "Myxobacteria: Moving, Killing, Feeding, and Surviving Together". In: *Frontiers in Microbiology* 7 (2016). DOI: 10.3389/fmicb.2016.00781.

[7] J. E. Berleman et al. "Predataxis behavior in *Myxococcus xanthus*". In: *Proceedings of the National Academy of Sciences* 105.44 (2008). DOI: 10.1073/pnas.0804387105.

[8] J. Pérez et al. "Rhizobial galactoglucan determines the predatory pattern of Myxococcus xanthus and protects Sinorhizobium meliloti from predation". In: *Environmental Microbiology* 16.7 (2014). DOI: 10.1111/1462-2920.12477.

[9] S. Thiery and C. Kaimer. "The Predation Strategy of Myxococcus xanthus". In: *Frontiers in Microbiology* 11 (2020). DOI: 10.3389/fmicb.2020.00002.

[10] S. Thiery et al. "The predatory soil bacterium Myxococcus xanthus combines a Tad- and an atypical type 3-like protein secretion system to kill bacterial cells". In: *Cell Reports* 40.11 (2022). DOI: 10.1016/j.celrep.2022.111340.

[11] W. Zhang et al. "Dynamics of Solitary Predation by Myxococcus xanthus on Escherichia coli Observed at the Single-Cell Level". In: *Applied and Environmental Microbiology* 86.3 (2020). Ed. by H. Nojiri. DOI: 10.1128/AEM.02286-19.

[12] S. Seef et al. "A Tad-like apparatus is required for contact-dependent prey killing in predatory social bacteria". In: *eLife* 10 (2021). DOI: 10.7554/eLife.72409.

[13] E. Rosenberg, K. H. Keller, and M. Dworkin. "Cell density-dependent growth of Myxococcus xanthus on casein". In: *Journal of Bacteriology* 129.2 (1977). DOI: 10.1128/jb.129.2.770-777.1977.

[14] B. D. Blackhart and D. R. Zusman. ""Frizzy" genes of Myxococcus xanthus are involved in control of frequency of reversal of gliding motility." In: *Proceedings of the National Academy of Sciences* 82.24 (1985). DOI: 10.1073/pnas.82.24.8767.

[15] M. Dworkin. "Tactic behavior of Myxococcus xanthus". In: *Journal of Bacteriology* 154.1 (1983). DOI: 10.1128/jb.154.1.452-459.1983.

[16] R. Mercier and T. Mignot. "Regulations governing the multicellular lifestyle of Myxococcus xanthus". In: *Current Opinion in Microbiology* 34 (2016). DOI: 10.1016/j.mib.2016.08.009.

[17] M. Dworkin and D. Eide. "*Myxococcus xanthus* Does Not Respond Chemotactically to Moderate Concentration Gradients". In: *Journal of Bacteriology* 154.1 (1983). DOI: 10.1128/jb.154.1.437-442.1983.

[18] H. Bloch et al. "Modelling, analysis, and simulation of traffic jam in colonies of Myxococcus xanthus (In preparation)". In: *In preparation* (2023).

[19] R. A. Fisher. "The wave of advance of advantageous genes". In: *Annals of Eugenics* 7.4 (1937). DOI: 10.1111/j.1469-1809.1937.tb02153.x.

[20] A. Kolmogorov. "Étude de l'équation de la diffusion avec croissance de la quantité de matière et son application à un problème biologique". In: *Moscow Univ. Bull. Math.* 1 (1937).

[21] A. Okubo. "Diffusion and ecological problems: mathematical models". In: *Biomath* 10 (1980). Publisher: Springer-Verlag.

[22] H. G. Othmer and S. Levin, eds. *Nonlinear Oscillations in Biology and Chemistry*. Vol. 66. Lecture Notes in Biomathematics. Berlin, Heidelberg: Springer Berlin Heidelberg, 1986. DOI: 10.1007/978-3-642-93318-9.

[23] E. E. Holmes. "Are Diffusion Models too Simple? A Comparison with Telegraph Models of Invasion". In: *The American Naturalist* 142.5 (1993). DOI: 10.1086/285572.

[24] T. Hillen. "Hyperbolic models for chemosensitive movement". In: *Mathematical Models and Methods in Applied Sciences* 12.07 (2002). DOI: 10.1142/S0218202502002008.

[25] J. A. Carrillo et al. "Double milling in self-propelled swarms from kinetic theory". In: *Kinetic & Related Models* 2.2 (2009). DOI: 10.3934/krm.2009.2.363.

[26] J. A. Carrillo, R. Eftimie, and F. K. O. Hoffmann. *Non-local kinetic and macroscopic models for self-organised animal aggregations*. Version Number: 1. 2014. DOI: 10.48550/ARXIV.1407.2099.

[27] Lutscher and Stevens. "Emerging Patterns in a Hyperbolic Model for Locally Interacting Cell Systems". In: *Journal of Nonlinear Science* 12.6 (2003). DOI: 10.1007/s00332-002-0510-4.

[28] T. Hillen and A. Stevens. "Hyperbolic models for chemotaxis in 1-D". In: *Nonlinear Analysis: Real World Applications* 1.3 (2000). DOI: 10.1016/S0362-546X(99)00284-9.

[29] J. Saragosti et al. "Directional persistence of chemotactic bacteria in a traveling concentration wave". In: *Proceedings of the National Academy of Sciences* 108.39 (2011). DOI: 10.1073/pnas.1101996108.

[30] A. Manhart. "Counter-propagating wave patterns in a swarm model with memory". In: *Journal of Mathematical Biology* 78.3 (2019). DOI: 10.1007/s00285-018-1287-x.

[31] M. Kac. "A stochastic model related to the telegrapher's equation". In: *The Rocky Mountain Journal of Mathematics* 4.3 (1974). Publisher: JSTOR.

[32] V. Calvez et al. “Regime switching on the propagation speed of travelling waves of some size-structured Myxobacteriapopulation models”. In: *In preparation* (2023).

[33] M. Estavoyer and T. Lepoutre. “Travelling waves for a fast reaction limit of a discrete coagulation–fragmentation model with diffusion and proliferation”. In: *Journal of Mathematical Biology* 89.1 (2024). DOI: 10.1007/s00285-024-02099-4.

[34] A. Gallegos, B. Mazzag, and A. Mogilner. “Two continuum models for the spreading of myxobacteria swarms”. In: *Bulletin of Mathematical Biology* 68.4 (2006). DOI: 10.1007/s11538-005-9031-2.

[35] P. Patra et al. “Colony Expansion of Socially Motile Myxococcus xanthus Cells Is Driven by Growth, Motility, and Exopolysaccharide Production”. In: *PLOS Computational Biology* 12.6 (2016). Ed. by C. V. Rao. DOI: 10.1371/journal.pcbi.1005010.

[36] K. P. Hadeler. “Hyperbolic travelling fronts”. In: *Proceedings of the Edinburgh Mathematical Society* 31.1 (1988). DOI: 10.1017/S001309150000660X.

[37] V. Méndez and J. Camacho. “Dynamics and thermodynamics of delayed population growth”. In: *Physical Review E* 55.6 (1997). DOI: 10.1103/PhysRevE.55.6476.

[38] S. Fedotov. *Traveling waves in reaction-diffusion system.* arXiv:cond-mat/9807352. 1998.

[39] K. P. Hadeler. “Reaction transport systems in biological modelling”. In: *Mathematics Inspired by Biology.* Ed. by V. Capasso. Vol. 1714. Series Title: Lecture Notes in Mathematics. Berlin, Heidelberg: Springer Berlin Heidelberg, 1999. DOI: 10.1007/BFb0092376.

[40] V. Méndez, J. Fort, and J. Farjas. “Speed of wave-front solutions to hyperbolic reaction-diffusion equations”. In: *Physical Review E* 60.5 (1999). DOI: 10.1103/PhysRevE.60.5231.

[41] B. Gilding and R. Kersner. “Wavefront solutions of a nonlinear telegraph equation”. In: *Journal of Differential Equations* 254.2 (2013). DOI: 10.1016/j.jde.2012.09.007.

[42] E. Bouin, V. Calvez, and G. Nadin. “Hyperbolic traveling waves driven by growth”. In: *Mathematical Models and Methods in Applied Sciences* 24.06 (2014). arXiv:1110.3242 [math]. DOI: 10.1142/S0218202513500802.

[43] V. Méndez, D. Campos, and W. Horsthemke. “Growth and dispersal with inertia: Hyperbolic reaction-transport systems”. In: *Physical Review E* 90.4 (2014). DOI: 10.1103/PhysRevE.90.042114.

[44] E. Barbera, C. Currò, and G. Valenti. “On discontinuous travelling wave solutions for a class of hyperbolic reaction–diffusion models”. In: *Physica D: Nonlinear Phenomena* 308 (2015). DOI: 10.1016/j.physd.2015.06.011.

[45] E. Barbera and G. Valenti. “Wave features of a hyperbolic reaction–diffusion model for Chemotaxis”. In: *Wave Motion* 78 (2018). DOI: 10.1016/j.wavemoti.2018.02.004.

[46] W. Van Saarloos. “Front propagation into unstable states”. In: *Physics Reports* 386.2-6 (2003). DOI: 10.1016/j.physrep.2003.08.001.

[47] S. Rombouts et al. “Multi-scale dynamic imaging reveals that cooperative motility behaviors promote efficient predation in bacteria”. In: *Nature Communications* 14.1 (2023). DOI: 10.1038/s41467-023-41193-x.

[48] H. F. Weinberger, M. A. Lewis, and B. Li. "Anomalous spreading speeds of cooperative recursion systems". In: *Journal of Mathematical Biology* 55.2 (2007). DOI: 10.1007/s00285-007-0078-6.

[49] M. Holzer and A. Scheel. "Criteria for Pointwise Growth and Their Role in Invasion Processes". In: *Journal of Nonlinear Science* 24.4 (2014). DOI: 10.1007/s00332-014-9202-0.

[50] M. Holzer. "A proof of anomalous invasion speeds in a system of coupled Fisher-KPP equations". In: (2014). Publisher: arXiv Version Number: 2. DOI: 10.48550/ARXIV.1409.8641.

[51] M. Holzer. "Anomalous spreading in a system of coupled Fisher–KPP equations". In: *Physica D: Nonlinear Phenomena* 270 (2014). DOI: 10.1016/j.physd.2013.12.003.

[52] G. Faye and G. Peltier. "Anomalous invasion speed in a system of coupled reaction-diffusion equations". In: *Communications in Mathematical Sciences* 16.2 (2018). DOI: 10.4310/CMS.2018.v16.n2.a7.

[53] F. Filbet and S. Jin. "A class of asymptotic preserving schemes for kinetic equations and related problems with stiff sources". In: *Journal of Computational Physics* 229.20 (2010). arXiv:0905.1378 [math]. DOI: 10.1016/j.jcp.2010.06.017.

[54] B. Després and F. Lagoutière. "Un schéma non linéaire anti-dissipatif pour l'équation d'advection linéaire". In: *Comptes Rendus de l'Académie des Sciences - Series I - Mathematics* 328.10 (1999). DOI: 10.1016/S0764-4442(99)80301-2.

[55] R. Leveque and H. Yee. "A study of numerical methods for hyperbolic conservation laws with stiff source terms". In: *Journal of Computational Physics* 86.1 (1990). DOI: 10.1016/0021-9991(90)90097-K.

[56] C. Lattanzio et al. *Analysis and numerics of the propagation speed for hyperbolic reaction-diffusion models*. arXiv:2206.09714 [cs, math]. 2022.

[57] M. Holzer and A. Scheel. "A slow pushed front in a Lotka–Volterra competition model". In: *Nonlinearity* 25.7 (2012). DOI: 10.1088/0951-7715/25/7/2151.

[58] A. M. Spormann. "Gliding Motility in Bacteria: Insights from Studies of *Myxococcus xanthus*". In: *Microbiology and Molecular Biology Reviews* 63.3 (1999). DOI: 10.1128/MMBR.63.3.621-641.1999.

[59] J. S. Mattick. "Type IV Pili and Twitching Motility". In: *Annual Review of Microbiology* 56.1 (2002). DOI: 10.1146/annurev.micro.56.012302.160938.

[60] D. Kaiser and C. Crosby. "Cell movement and its coordination in swarms of myxococcus xanthus". In: *Cell Motility* 3.3 (1983). DOI: 10.1002/cm.970030304.

[61] M. Avery, M. Holzer, and A. Scheel. "Pushed-to-Pulled Front Transitions: Continuation, Speed Scalings, and Hidden Monotonicty". In: *Journal of Nonlinear Science* 33.6 (2023). DOI: 10.1007/s00332-023-09957-3.

[62] S. Müller et al. "Bacillaene and Sporulation Protect Bacillus subtilis from Predation by Myxococcus xanthus". In: *Applied and Environmental Microbiology* 80.18 (2014). Ed. by A. M. Spormann. DOI: 10.1128/AEM.01621-14.

[63] S. Müller et al. "Predation by Myxococcus xanthus Induces Bacillus subtilis To Form Spore-Filled Megastructures". In: *Applied and Environmental Microbiology* 81.1 (2015). Ed. by M. A. Elliot. DOI: 10.1128/AEM.02448-14.

[64] W. H. DePas et al. "Biofilm Formation Protects Escherichia coli against Killing by Caenorhabditis elegans and Myxococcus xanthus". In: *Applied and Environmental Microbiology* 80.22 (2014). Ed. by H. Nojiri. DOI: 10.1128/AEM.02464-14.

[65] M. Vasse et al. "Killer prey: Ecology reverses bacterial predation". In: *PLOS Biology* 22.1 (2024). Ed. by L. Søgaard-Andersen. DOI: 10.1371/journal.pbio.3002454.

[66] L. J. Shimkets and D. Kaiser. "Induction of coordinated movement of Myxococcus xanthus cells". In: *Journal of Bacteriology* 152.1 (1982). DOI: 10.1128/jb.152.1.451-461.1982.

[67] B. Sager and D. Kaiser. "Intercellular C-signaling and the traveling waves of Myxococcus." In: *Genes & Development* 8.23 (1994). DOI: 10.1101/gad.8.23.2793.

[68] J. E. Berleman et al. "Rippling Is a Predatory Behavior in *Myxococcus xanthus*". In: *Journal of Bacteriology* 188.16 (2006). DOI: 10.1128/JB.00559-06.

[69] O. Sliusarenko et al. "Accordion waves in *Myxococcus xanthus*". In: *Proceedings of the National Academy of Sciences* 103.5 (2006). DOI: 10.1073/pnas.0507720103.

[70] D. Kaiser. "Signaling in myxobacteria". In: *Annual Review of Microbiology* 58.1 (2004). DOI: 10.1146/annurev.micro.58.030603.123620.

[71] K. A. O'Connor and D. R. Zusman. "Development in Myxococcus xanthus involves differentiation into two cell types, peripheral rods and spores". In: *Journal of Bacteriology* 173.11 (1991). DOI: 10.1128/jb.173.11.3318-3333.1991.

[72] O. A. Igoshin et al. "Pattern formation and traveling waves in myxobacteria: Theory and modeling". In: *Proceedings of the National Academy of Sciences* 98.26 (2001). DOI: 10.1073/pnas.221579598.

[73] O. A. Igoshin et al. "Waves and aggregation patterns in myxobacteria". In: *Proceedings of the National Academy of Sciences* 101.12 (2004). DOI: 10.1073/pnas.0400704101.

[74] R. Eftimie, G. De Vries, and M. A. Lewis. "Complex spatial group patterns result from different animal communication mechanisms". In: *Proceedings of the National Academy of Sciences* 104.17 (2007). DOI: 10.1073/pnas.0611483104.

[75] O. Sozinova et al. "A three-dimensional model of myxobacterial fruiting-body formation". In: *Proceedings of the National Academy of Sciences* 103.46 (2006). DOI: 10.1073/pnas.0605555103.

[76] O. Sliusarenko, D. R. Zusman, and G. Oster. "Aggregation during Fruiting Body Formation in *Myxococcus xanthus* Is Driven by Reducing Cell Movement". In: *Journal of Bacteriology* 189.2 (2007). DOI: 10.1128/JB.01206-06.

[77] A. Scheel and A. Stevens. "Wavenumber selection in coupled transport equations". In: *Journal of Mathematical Biology* 75.5 (2017). DOI: 10.1007/s00285-017-1107-8.

[78] R. Eftimie. "Hyperbolic and kinetic models for self-organized biological aggregations and movement: a brief review". In: *Journal of Mathematical Biology* 65.1 (2012). DOI: 10.1007/s00285-011-0452-2.

[79] V. Méndez, S. A. Fedotov, and W. Horsthemke. *Reaction-transport systems: mesoscopic foundations, fronts, and spatial instabilities*. Springer series in synergetics. Berlin Heidelberg: Springer, 2010.

[80] E. P. Zemskov and W. Horsthemke. "Diffusive instabilities in hyperbolic reaction-diffusion equations". In: *Physical Review E* 93.3 (2016). DOI: 10.1103/PhysRevE.93.032211.

[81] G. Consolo, C. Currò, and G. Valenti. "Pattern formation and modulation in a hyperbolic vegetation model for semiarid environments". In: *Applied Mathematical Modelling* 43 (2017). DOI: 10.1016/j.apm.2016.11.031.

[82] G. Consolo et al. "Oscillatory periodic pattern dynamics in hyperbolic reaction-advection-diffusion models". In: *Physical Review E* 105.3 (2022). DOI: 10.1103/PhysRevE.105.034206.

[83] C. Currò and G. Valenti. "Pattern formation in hyperbolic models with cross-diffusion: Theory and applications". In: *Physica D: Nonlinear Phenomena* 418 (2021). DOI: 10.1016/j.physd.2021.132846.

[84] J. S. Ritchie, A. L. Krause, and R. A. Van Gorder. "Turing and wave instabilities in hyperbolic reaction–diffusion systems: The role of second-order time derivatives and cross-diffusion terms on pattern formation". In: *Annals of Physics* 444 (2022). DOI: 10.1016/j.aop.2022.169033.

[85] G. Dee and J. S. Langer. "Propagating Pattern Selection". In: *Physical Review Letters* 50.6 (1983). DOI: 10.1103/PhysRevLett.50.383.

[86] W. Van Saarloos. "Front propagation into unstable states: Marginal stability as a dynamical mechanism for velocity selection". In: *Physical Review A* 37.1 (1988). DOI: 10.1103/PhysRevA.37.211.

[87] W. Van Saarloos. "Front propagation into unstable states. II. Linear versus nonlinear marginal stability and rate of convergence". In: *Physical Review A* 39.12 (1989). DOI: 10.1103/PhysRevA.39.6367.

[88] M. Avery and A. Scheel. "Universal selection of pulled fronts". In: *Communications of the American Mathematical Society* 2.5 (2022). DOI: 10.1090/cams/8.

[89] M. Avery. *Front selection in reaction-diffusion systems via diffusive normal forms*. arXiv:2211.11829 [nlin]. 2023.

[90] G. Faye, M. Holzer, and A. Scheel. "Linear spreading speeds from nonlinear resonant interaction". In: *Nonlinearity* 30.6 (2017). DOI: 10.1088/1361-6544/aa6c74.

[91] M. Avery et al. "Instability in large bounded domains—branched versus unbranched resonances". In: *Nonlinearity* 34.11 (2021). DOI: 10.1088/1361-6544/ac2a15.